

CANADIAN THESES ON MICROFICHE

I.S.B.N.

THESES CANADIENNES SUR MICROFICHE



National Library of Canada
Collections Development Branch

Bibliothèque nationale du Canada
Direction du développement des collections

Canadian Theses on
Microfiche Service

Service des thèses canadiennes
sur microfiche

Ottawa, Canada
K1A 0N4

NOTICE

The quality of this microfiche is heavily dependent upon the quality of the original thesis submitted for microfilming. Every effort has been made to ensure the highest quality of reproduction possible.

If pages are missing, contact the university which granted the degree.

Some pages may have indistinct print especially if the original pages were typed with a poor typewriter ribbon or if the university sent us a poor photocopy.

Previously copyrighted materials (journal articles, published tests, etc.) are not filmed.

Reproduction in full or in part of this film is governed by the Canadian Copyright Act, R.S.C. 1970, c. C-30. Please read the authorization forms which accompany this thesis.

THIS DISSERTATION
HAS BEEN MICROFILMED
EXACTLY AS RECEIVED

AVIS

La qualité de cette microfiche dépend grandement de la qualité de la thèse soumise au microfilmage. Nous avons tout fait pour assurer une qualité supérieure de reproduction.

S'il manque des pages, veuillez communiquer avec l'université qui a conféré le grade.

La qualité d'impression de certaines pages peut laisser à désirer, surtout si les pages originales ont été dactylographiées à l'aide d'un ruban usé ou si l'université nous a fait parvenir une photocopie de mauvaise qualité.

Les documents qui font déjà l'objet d'un droit d'auteur (articles de revue, examens publiés, etc.) ne sont pas microfilmés.

La reproduction, même partielle, de ce microfilm est soumise à la Loi canadienne sur le droit d'auteur, SRC 1970, c. C-30. Veuillez prendre connaissance des formules d'autorisation qui accompagnent cette thèse.

LA THÈSE A ÉTÉ
MICROFILMÉE TELLE QUE
NOUS L'AVONS REÇUE

**MORPHOMETRIC AND THREE-DIMENSIONAL RECONSTRUCTION ANALYSIS
OF VARIATIONS IN GUINEA PIG PHOTORECEPTOR
SYNAPTIC TERMINALS**

by

MITCHELL DAVID MCCARTNEY

Department of Anatomy
Dalhousie University
Halifax, Nova Scotia

"Submitted in partial fulfillment of the requirements of the
degree of Doctor of Philosophy at Dalhousie University,"
April 8, 1985.

© 1985 by Mitchell D. McCartney

Dedication

This thesis is dedicated to Dianne, Dad, Mum and Andy.

I only hope that I am able to provide the support, encouragement, understanding and love that I have received from them.

TABLE OF CONTENTS

	Page
Title Page	i
Signature Page	ii
Copyright Agreement Form	iii
Dedication	iv
Table of Contents	v
List of Illustrations	vii
Abstract	x
List of Abbreviations	xi
Acknowledgments	xiii
I INTRODUCTION	1
II MATERIAL AND METHODS	13
A. Experimental Animals	13
B. Lighting Conditions	
(i) Diurnal Cycle (L:D 12:12)	
(a) Adult	14
(b) Fetal	14
(c) Neonatal	15
(ii) Long-Term Light and Dark Adaptation	15
C. Tissue Preparation	16
D. Morphological Examination	
(i) Three-Dimensional Reconstruction	17
(ii) Morphometric Measurements	18
(iii) Numerical Density of Synaptic Vesicles	20

	Page
III RESULTS	23
A. Qualitative	
(i) Light Microscopy - Guinea Pig Retina	
(a) Adult	23
(b) Fetal and Neonatal	24
(ii) Electron Microscopy - Synaptic Terminals	25
B. Quantitative - Synaptic Terminals	
(i) Diurnal Lighting Effects - Adult	
(a) Morphometric Measurements	27
(b) Three-Dimensional Reconstructions	31
(ii) Long-Term Light and Dark Adaptation - Adult ...	32
(iii) Diurnal Lighting Effects - Fetal	34
(iv) Diurnal Lighting Effects - Neonatal	34
C. Quantitative - Synaptic Ribbons	
(i) Diurnal Lighting Effects - Adults	
(a) Three-Dimensional Reconstructions	35
(b) Morphometric Measurements	37
(ii) Long-Term Light and Dark Adaptation - Adult ...	38
(iii) Diurnal Lighting Effects - Fetal	39
(iv) Diurnal Lighting Effects - Neonatal	40
Figures	41
IV DISCUSSION	83
A. Photoreceptor Synaptic Terminals	85
B. Photoreceptor Synaptic Ribbons	98
V SUMMARY	104
REFERENCES	108
CURRICULUM VITAE	124

List of Illustrations

Figure		Page
1	Photograph of colour-coded synaptic terminal tracings on acetate sheets.	42
2	Diagram of template used for measurements of rod and cone synaptic terminals.	44
3	Light micrograph of the full thickness of the adult retina.	46
4	Light micrograph of the full thickness of the fetal retina.	46
5	Transmission electron micrograph of an alpha rod synaptic terminal.	49
6	Transmission electron micrograph of a paranuclear rod synaptic terminal.	49
7	Transmission electron micrograph of a cone synaptic terminal.	49
8	Transmission electron micrograph of a cone synaptic ribbon.	49
9	Transmission electron micrograph of an alpha rod synaptic terminal.	51
10	Transmission electron micrograph of a paranuclear rod synaptic terminal.	51
11	Transmission electron micrograph of a cone synaptic terminal.	51
12	Transmission electron micrograph of a cross-striated fibril.	51
13	Graphs showing the relationship between synaptic terminal profile area and sample time over a 24-hr cycle.	54
14	Graphs showing the relationship between synaptic terminal profile form factor and sample time over a 24-hr cycle.	54
15	Graphs showing the relationship between synaptic terminal profile perimeter and sample time over a 24-hr cycle.	54

Figure

Page

16	Graphs showing the relationship between synaptic vesicle diameter and sample time over a 24-hr cycle.	57
17	Graphs showing the relationship between the number of synaptic vesicles per μm^2 and sample time over a 24-hr cycle.	57
18	Graphs showing the relationship between the number of synaptic vesicles per terminal profile and sample time over a 24-hr cycle.	57
19	Transmission electron micrographs of the synaptic terminals of an alpha and paranuclear rod and a cone.	60
20	Three-dimensional reconstructions of an alpha and paranuclear rod and a cone from the light period of a diurnal cycle.	60
21	Three-dimensional reconstructions of an alpha and paranuclear rod and a cone from the dark period of a diurnal cycle.	60
22	Histograms comparing terminal area values obtained in diurnal and extended lighting conditions.	62
23	Graphs showing the relationship between fetal synaptic profile area and sample time over a 24-hr cycle.	64
24	Graphs showing the relationship between fetal synaptic terminal profile form factor and sample time over a 24-hr cycle.	64
25	Graphs showing the relationship between fetal synaptic terminal profile perimeter and sample time over a 24-hr cycle.	64
26	Histograms comparing the neonatal terminal profile area and two sample times during a diurnal cycle.	66
27	Three-dimensional reconstructions of an alpha rod synaptic terminal and its synaptic ribbon.	68
28	Three-dimensional reconstructions of a cone synaptic terminal and its synaptic ribbons.	68

Figure		Page
29	Three-dimensional reconstructions of an alpha rod and its synaptic ribbon (including stereo pair).	70
30	Three-dimensional reconstructions of an alpha rod and its synaptic ribbon (including stereo pair).	70
31	Three-dimensional reconstructions of an alpha rod synaptic ribbon and its related postsynaptic elements.	72
32	Three-dimensional reconstructions of an alpha rod.	74
33	Graphs showing the relationship between synaptic ribbon length and sample time, and between the number of synaptic ribbons per terminal profile and sample time over a 24-hr cycle.	76
34	Histograms showing the relationship between adult synaptic ribbon length and sample time, and between the number of synaptic ribbons per terminal profile and sample time in animals exposed to extended lighting conditions.	78
35	Graphs showing the relationship between fetal synaptic ribbon length and sample time, and between the number of synaptic ribbons per terminal profile and sample time over a 24-hr cycle.	80
36	Histograms showing the relationship between neonatal synaptic ribbon length and sample time, and between the number of synaptic ribbons per terminal profile and sample time during a diurnal cycle.	82

ABSTRACT

In order to test whether reported alterations in photoreceptor synaptic terminals occur in a mammalian visual system, adult, fetal and neonatal guinea pig retinas were exposed to a 12:12 L:D diurnal lighting cycle, as well as to long-term light (L:L) and long-term dark (D:D) regimes. Representative samples from all retinal quadrants, obtained at various times throughout the lighting regimes, were processed for electron microscopy and the synaptic terminals of all three photoreceptor cell types found in this retina (alpha and paranuclear rods, and cones) were analysed using computer-assisted morphometrics for changes in their area, perimeter, synaptic vesicle numerical density, the degree of plasmalemmal infolding, as well as for synaptic ribbon length and absolute number per terminal. Diurnal data showed that all three types of adult photoreceptors have increased synaptic terminal areas and greater synaptic vesicle numerical density, as well as decreased terminal membrane infolding, during the light period, while both types of rods showed increased perimeter measurements in the dark. Results from adults maintained in extended lighting conditions showed no difference between these sample times even though statistically significant differences existed in diurnal data. Alternatively, diurnal data from fetal and neonatal retinas showed no significantly sustainable pattern in any of these synaptic terminal parameters. Similarly, synaptic ribbon length and number per terminal profile exhibited no statistically significant change throughout diurnal or extended lighting conditions, in adult, fetal or neonatal retinas. These quantitative findings, have led to the conclusion that, although alterations in synaptic terminal perimeter measurements may be explained using the vesicle recycling hypothesis, changes in terminal size and shape may be effected by an annular configuration of cross-striated fibrils found within these receptor terminals. Further, computer-assisted morphometrics and 3-D reconstruction analyses have shown that synaptic ribbon length and number per terminal profile does not change in guinea pig photoreceptor synaptic terminals.

List of Abbreviations

ATPase	Adenosinetriphosphatase
b	Bipolar cell
BMDP	BMDP Biomedical Computer Programs
CDC	Control Data Corporation
D:D	Dark:Dark
o	Degrees
OC	Degrees Celsius
ELM	External limiting membrane
ft-c	Foot candle
GC	Ganglion cell layer
g	Gram
h	Horizontal cell
hl	A second horizontal cell
HRP	Horseradish peroxidase
hr	hour
INL	Inner nuclear layer
IPL	Inner plexiform layer
ILM	Internal limiting membrane
kg	Kilogram
l	Length
L:D	Light:Dark
L:L	Light:Light
DQ	Mean diameter
D	Mean particle diameter
µm	Micrometer

μm^2	Square micrometer
mg	Milligram
mm	Millimeter
mM	Millimolar
mOsm	Milliosmole
min	Minute
M	Molar
nm	Nanometer
n	Nucleus
Na	Number of particles in AT
Nv	Numerical particle density
NFL	Optic nerve fiber layer
OsO ₄	Osmium tetroxide
ONL	Outer nuclear layer
OPL	Outer plexiform layer
PE	Pigment epithelium
RCS	Rod and cone outer and inner segments
s	Section s
s'	Section s'
s''	Section s''
t	Section thickness
SER	Smooth endoplasmic reticulum
S.E.M.	Standard error of the mean
SR	Synaptic ribbon
AT	Sum of reference areas
wk	Week
w	Width

Acknowledgments

I would like to express my appreciation to my supervisor, Dr. D.H. Dickson, for his support, guidance and patience. I am proud to be able to refer to him as my friend and colleague.

I would also like to extend my appreciation to Dr. D.G. Gwyn, Professor and Head of the Department of Anatomy, for making microscopical and laboratory facilities available to me. I am also grateful to Mr. George Robertson and Mr. Michael Moyles for their valuable technical assistance.

Finally, I would like to thank all of my friends and colleagues in the Department of Anatomy for all of their advice and assistance during my time at Dalhousie. Although too numerous to acknowledge individually, I hope they realize how much I appreciated their help.

This investigation was supported by a grant from the Medical Research Council of Canada to Dr. D.H. Dickson. The author received personal support from the Faculty of Graduate Studies, Dalhousie University, and from the Medical Research Council of Canada. The author wishes to express his appreciation to these organizations for their financial support.

I. INTRODUCTION

A variety of different lighting conditions have been reported to cause alterations in the size and shape of photoreceptor synaptic terminals (Ball and Dickson, 1983; Cooper and McLaughlin, 1982; Cooper, McLaughlin and Boykins, 1983; Shaeffer and Raviola, 1976; 1978), in the length and number of synaptic ribbons within terminals (Grun, 1980; Spadaro, de Simone and Puzzolo, 1978; Wagner, 1973; Wagner and Ali, 1977) and in the relationship between presynaptic and postsynaptic elements (Ball and Dickson, 1983; Brandon and Lam, 1983; Raynauld, Lavoilette and Wagner, 1979; Schaeffer and Raviola, 1976; Wagner, 1980). The majority of these reported changes have been shown to occur in lower vertebrates and accordingly the universality of these phenomena is open to speculation.

In order to obtain reliable quantitative data from a mammalian visual system, the present study was undertaken using the guinea pig as a model. The guinea pig is similar to primates, in that it has been shown to have a fully developed retina before birth (Spira, 1975). Spira (1975) showed that the differentiation of the neural retina commences around the twenty-third day of gestation and is

fully developed between the fifty-first and the fifty-seventh day of an average 63-day gestation period (Draper, 1920). Based on the differentiation of the fetal retina into ten histologically identifiable layers, the presence of ribbon synapses in the outer plexiform layer and fully developed photoreceptor inner and outer segments, Spira (1975) concluded that the fetal guinea pig retina was functionally mature in utero. Additional evidence for this functional maturity comes from reports that the outer segment tips of fetal guinea pig photoreceptors are not only shed in utero (Spira and Huang, 1978), but also that this shedding follows a cyclic pattern similar to the one found in adult guinea pig retinas (Huang, Spira and Wyse, 1982). Further studies by Huang, Spira and Wyse (1983) suggest that this fetal outer segment shedding is regulated in a manner independent from the shedding cycle of the adult. Accordingly, it is the hypothesis of the present study that if alterations in photoreceptor synaptic terminals occur in the adult, they should be evident in fetal guinea pigs as well.

The photoreceptors in the retina of the guinea pig were one of the first cell types to be examined using transmission electron microscopy. In this classic study, Sjöstrand (1953) described two types of photoreceptor cells. The first having a nucleus in the vitreal portion of the outer nuclear layer (ONL) and a triad of postsynaptic invaginations in its synaptic terminal, he designated an

alpha rod. The nucleus of the second photoreceptor type was located in the scleral portion of the ONL and the synaptic terminals of these cells were characterized by multiple postsynaptic invaginations. These latter cells he termed beta rods; however, on the basis of morphological and physiological criteria used today, they should more correctly be termed cones (Huang et al., 1982; Schmalenberger, 1980). Further studies by Mountford (1963) revealed that, in addition to the two receptor types outlined by Sjöstrand (1953), there existed as well, a third cell type which she called a paranuclear rod. It had similar morphological characteristics to the alpha rod, except that the nucleus was in close proximity to the invaginations of the postsynaptic elements. All three photoreceptor cell types were later identified by Spira (1975) in the fetal guinea pig retina.

Sjöstrand (1953) was also the first to report the occurrence of a cross-striated fibril within the inner segment of the guinea pig rod, and extending towards the outer limiting membrane. This cross-striated fibril was observed to originate near, or from the pair of centrioles in the apex of the inner segment. A detailed account of the extent of this unusual ciliary rosette was subsequently given by Spira and Milman (1979). They described this structure as an aggregate of thin cross-striated filaments which extends from the inner segment region, through the full length of the cell body and terminates in the synaptic

terminal. This demonstrated extension of the cross-striated filament into the synaptic terminal explains the previous observation of a "synaptic spindle" by Mountford (1964). Cross-striated filaments are not unique to the guinea pig; they have been noted in the retina of the developing and mature mouse (Olney, 1968), adult cat (Stevens, Jacobs and Jackson, 1984) and in man (Uga, Nakao, Mimura and Ikui, 1970; Villegas, 1964). Although the function of this organelle is still a matter of conjecture, the presence of actin and myosin-like immunoreactivity in rat inner segments (Drenckhahn and Groschel-Stewart, 1977), the localization of ATPase in the inner segment of human rods (Matsusaka, 1967) and ATPase localization along the entire extent of the fibril in guinea pig photoreceptors (Spira and Milman, 1982), has led to the suggestion that these fibrils may be contractile. In the cat, serially-reconstructed cross-striated fibrils from cone terminals (Stevens et al., 1984) were shown to be arranged in a ring-like configuration, surrounding synaptic ribbons and invaginating postsynaptic elements. This arrangement has led Stevens et al. (1984) to suggest that this organelle may be responsible for documented alterations in the size and shape of photoreceptor synaptic terminals (Ball and Dickson, 1983; Cooper and McLaughlin, 1982; Cooper et al., 1983; Schaeffer and Raviola, 1976; 1978). This is however contrary to previous studies where synaptic terminal alterations have been associated with the exocytosis and endocytosis

(recycling) of synaptic vesicle membrane at the terminal plasma membrane.

Following the demonstration that acetylcholine was released as discrete quantal packets (Fatt and Katz, 1952) and the electron microscopic observation of synaptic vesicles within synaptic terminals (De Robertis and Bennett, 1954; Palade, 1954; Palay, 1954), Del Castillo and Katz (1955) suggested that transmitter release was effected through vesicle exocytosis. More recent studies have provided additional evidence for the fusion of synaptic vesicles with the presynaptic membrane (Heuser and Reese, 1973; Heuser, Reese, Dennis, Jan, Jan and Evans, 1979; Zimmerman, 1978; 1979a, b) and with the complete incorporation of the vesicle membrane into the terminal plasmalemma (Heuser and Reese, 1980).

It is now generally accepted that the mechanism of transmitter release through synaptic vesicle exocytosis, is coupled with endocytosis, and that this second phenomenon is usually observed in close proximity to the synaptic site. Although endocytosis has been demonstrated extensively at neuromuscular junctions (Miller and Heuser, 1984), more relevant to the present study, it has also been shown to occur actively in dark-adapted retinal photoreceptor synaptic terminals (Ball and Dickson, 1983; Cooper and McLaughlin, 1982; Cooper et al., 1983; Brandon and Lam, 1983). As further proof for the existence of this phenomenon, a number of studies, using a variety of

vertebrates, have demonstrated uptake of the extracellular tracer horseradish peroxidase (HRP) into photoreceptor synaptic vesicles in the dark (Cooper and McLaughlin, 1983; Ripps, Shakib and MacDonald, 1976; Schacher, Holtzman and Hood, 1974; 1976; Schaeffer and Raviola, 1976). These authors reasoned that since this activity was absent or greatly reduced in the light, membrane retrieval via exocytosis must be occurring concurrently with synaptic vesicle fusion. Further, morphological evidence has suggested that this retrieval is mediated both by coated vesicles (Ball and Dickson, 1983; Cooper and McLaughlin, 1983; Schaeffer and Raviola, 1976), and by uncoated vesicles, at active zones of the photoreceptor synaptic terminal plasmalemma (Cooper and McLaughlin, 1983, Cooper et al., 1983).

Evidence for exocytotic release of transmitter and the subsequent retrieval of vesicle membrane by endocytosis led Heuser and Reese (1973) to suggest the vesicle recycling hypothesis. While this proposal is still disputed by some authors (Dunant and Israel, 1979; Marchbanks, 1978; 1979) who argue that exocytosis does not account for transmitter release and that synaptic vesicles more likely represent storage depots for the cytoplasmic pool of transmitter, or for calcium, many authors (see review by Holtzman and Mercurio, 1980) believe that the vesicle recycling hypothesis presents an attractive solution to account for the fate of membrane in synaptic terminals. Briefly, the

vesicle hypothesis states that during transmitter release, synaptic vesicles fuse with the presynaptic membrane; membrane is then internalized as coated vesicles which subsequently lose their clathrin coats and fuse with the saccules of the smooth endoplasmic reticulum (SER). These membrane additions to the SER result in the formation of enlarged cisternae, which in turn give birth to new synaptic vesicles. Heuser and Reese (1973) termed this sequence of events, the exo-endocytotic cycle, and this has formed the basis of arguments for explaining the changes in size and shape of photoreceptor synaptic terminals which have been demonstrated in a variety of vertebrates (Ball and Dickson, 1983; Brandon and Lam, 1983; Cooper and McLaughlin, 1982; Raynauld et al., 1979; Schaeffer and Raviola, 1976; 1978; Wagner, 1980).

Many of the changes that have been reported in photoreceptor synaptic terminals have also been observed in retinas exposed to extremes of temperature or light.

Schaeffer and Raviola (1976, 1978), for example, demonstrated increased terminal sizes in turtle photoreceptors when the animals were maintained at 4°C. They suggested that the lowered body temperature inhibited the membrane retrieval process resulting in an increase in terminal size as synaptic vesicle membrane was added to the plasmalemma during vesicle exocytosis.

A variety of morphological changes have also been reported to occur on an ongoing basis in normal, diurnally

entrained animals. Cooper and McLaughlin (1982) and Cooper et al. (1983) have provided evidence to suggest that, in chick photoreceptor synaptic terminals exposed to a 12:12 L:D lighting cycle, membrane diverticula are created to serve as 'storage areas' for membrane added during transmitter release. These multiple membrane domains were noted at various times throughout the lighting cycle, and the authors suggest that they disappear when the stored membrane is recycled into synaptic vesicles. Ball and Dickson (1983) also reported cyclic alterations in the synaptic terminals of aquatic newts exposed to a 12:12 L:D diurnal lighting cycle. In their study, the photoreceptor synaptic terminals became significantly larger in area late in the dark part of the cycle, suggesting that additional membrane was being incorporated into the plasmalemma, due possibly to an increased rate of vesicle exocytosis at this time. Similar to Osborne and Monaghan (1976) and Cooper and McLaughlin (1982), Ball and Dickson (1983) observed dense-cored vesicles in receptor synaptic terminals near the end of the light period. In addition, they also supported the suggestion of Osborne and Monaghan (1976), that in the light, synaptic vesicles may have the opportunity to become "supercharged" with transmitter as evidenced by the increased number of dense-cored vesicles.

Fluctuations in the physical relationship between the photoreceptor synaptic terminal and the invaginating postsynaptic elements have also been reported. Brandon and

Lam (1983) observed an increase, during the dark, in the amount of photoreceptor plasmalemma in the rat following a period of active vesicle fusion, but suggested that this membrane addition, together with the subsequent evagination of the terminal plasmalemma, is localized to the area adjacent to the postsynaptic horizontal cell processes. Further, they suggested that this localized addition and subsequent retrieval of membrane occurs only in rod synaptic terminals. Raynauld et al. (1979) and Wagner (1980), however, noted an increase in finger-like extensions of invaginating horizontal cell processes of the goldfish in the light-adapted state. These structures, which they called spinules, almost completely disappeared after dark adaptation. Dark-adapted retinas also are reported (Schaeffer and Raviola, 1976) to have an increased ratio of synaptic contact area (photoreceptor plasmalemma adjacent to the invaginating processes of bipolar and horizontal cells) over areas of non-synaptic contact (remainder of the photoreceptor terminal membrane).

To date, attempts to quantify reported morphological changes in photoreceptor synaptic terminals have been limited. De Robertis and Franchi (1956) were the first to attempt to quantify morphological alterations in photoreceptor synaptic terminals when they suggested that the terminals of albino rabbits kept in the dark for nine days contained smaller vesicles than those terminals from animals sampled in the light. These findings were later

disputed by Mountford (1963) who, following statistical analysis of the vesicle populations, concluded that the vesicle size did not vary significantly between samples obtained in the light and in the dark. Cragg (1969) supported the findings of Mountford (1963), when he found no change in synaptic vesicle diameter in newborn rat photoreceptor synaptic terminals sampled in the light and in the dark. However, he did report an apparent greater number of vesicles within terminals, as well as a decrease in terminal width during the light period of a diurnal cycle. When taken together, these findings led him to suggest that the actual number of vesicles per synaptic terminal had not changed, but rather the synaptic vesicle density varied according to the changing terminal size. This concept of steady-state synaptic terminal vesicle population size has recently been confirmed in the retina of an aquatic newt, Notophthalmus, as well (Ball and Dickson, 1983).

Perhaps the most controversial quantitative studies to be carried out on photoreceptor synaptic terminals have been those dealing with synaptic ribbons. Synaptic ribbons are organelles, which appear in thin sections as electron-dense lamellar structures, and have been known by a variety of names, including membrane processes (DeRobertis and Franchi, 1956), synaptic lamellae (Cohen, 1960; Fine, 1962; Ladman, 1958) and synaptic ribbons (Sjöstrand, 1958). Although the function of synaptic ribbons (lamellae) is as yet unconfirmed, they have been suggested to subservise in the

maintenance of synaptic terminal membrane shape, as well as having an orienting effect on the synaptic vesicles within the terminal (Bunt, 1971), or possibly to function as storage sites for transmitter substances (Osborne and Thornhill, 1972).

Synaptic ribbons have also been reported to undergo morphological alterations in response to lighting conditions. In fish, Wagner (1973) and Wagner and Ali (1977) reported a reduction in synaptic ribbon numbers in cones during the dark portion of a light:dark cycle; however, no change in ribbon number was observed in rod synaptic terminals. Alternatively, Spadaro et al. (1978) reported a decrease in rat rod and cone ribbon numbers in the dark. In addition to variation in the number of synaptic ribbons, a reduction in their length has also been reported in a cichlid fish and the African claw-toed frog, Xenopus, during the dark part of the diurnal cycle (Grun, 1980), while Spadaro et al. (1978) noted a shortening in synaptic ribbon length during the light portion of the cycle in both the rods and cones of the albino rat.

To date, precise quantitative analyses of diurnal variation in photoreceptor synaptic terminal size and shape, synaptic ribbon length and synaptic ribbon numbers have, for the most part, been inadequate either from a sampling or from a statistical standpoint. Therefore, in order to more accurately quantify any of these variations that might be

occurring in adult, fetal and neonatal guinea pig retinas exposed to a normal 12:12 diurnal (L:D) lighting cycle, as well as in tissue from long-term light (L:L) and long-term dark (D:D) adapted adult animals, the present study has employed rigid sampling criteria, coupled with morphometric and computer assisted three-dimensional reconstruction analysis.

II. MATERIALS AND METHODS

A. Experimental Animals

Adult Hartley-outbred guinea pigs (High Oaks Farms, Oakville, ON) were housed in rack cages, given food and water ad libitum and entrained to a 12 hr light:12 hr dark diurnal lighting regime for at least 2 wk prior to the initiation of experiments.

In order to ensure a continual supply of accurately timed fetal animals, sexually mature adults were obtained and a breeding colony established. The time of mating was estimated by allowing a male to be in contact with females for a single 24-hr period, after which the females were housed separately. These females were then checked, by palpation, at regular intervals to establish if they were pregnant. In addition to this method of age determination from mating times, the criteria established by Draper (1920) based on crown to rump measurements, were used to confirm fetal age at the time of sacrifice.

Neonatal animals were obtained from breeding colony stock. When a pregnant sow was nearing the end of term, she was carefully monitored to establish the time of birth of the pups. Since the 'normal' time of birth is during the

dark period of the diurnal cycle, pups were stated to be 1 day of age during their first light period.

B. Lighting Conditions

(i) Diurnal Cycle (L:D 12:12)

(a) Adult

Pregnant females (at approximately the 62nd day of their pregnancy), as well as male and non-pregnant female guinea pigs weighing approximately 800 g, were anesthetized with Somnotol (M.T.C. Pharmaceuticals, Hamilton, ON) at a dosage of 60 mg/kg body weight, at ten times throughout the 24-hr light:dark cycle, and their eyes were enucleated. Those animals sampled during the light period of the cycle had their eyes removed under ambient room lighting conditions, with an illumination of approximately 110 ft-c. In the dark period, eyes were removed with the aid of an infrared intensifying viewer (Metascope model 9902 E/A, Varo Inc., Garland, TX). A minimum of two adult animals were sampled at each sample time. Additional adult animals were sampled at critical times, bringing the total to four animals at 1830 and 2000, while five (total) animals were sampled at 0600 and 0800 respectively.

(b) Fetal

Fetal specimens were obtained at the same time that eyes were removed from pregnant females, and under the same lighting conditions. Once the fetuses were removed from the

sow, they were anesthetized with Somnotol at a dosage of 60 mg/kg body weight.

(c) Neonatal

Neonatal animals were anesthetized (Somnotol; 60 mg/kg body weight) and sampled at 1300 (light) and 0230 (dark) during a 12:12 L:D cycle. These sample times were chosen as representative times in the centre of the lighting periods (L:D).

According to the aging criteria established in Materials and Methods, Section A, animals that were 1, 3, 5, and 7 days of age were used. At each sample time, at least two animals from each group were sacrificed.

(ii) Long-Term Light and Dark Adaptation

Adult animals that had previously been entrained to a diurnal cycle, were exposed to long-term light or alternatively long-term dark adaptation. These animals were housed in rack cages in either continual light or darkness.

After periods of two days, one and two weeks in continuous light or dark, samples were taken at 0600 and 0800. Sampling times were based on data previously obtained from adult animals exposed to a diurnal lighting cycle (see Section B, i, a above). Eyes obtained in the light were removed under ambient room lighting conditions, while those obtained in the dark were enucleated in the dark as above.

C. Tissue Preparation

Once removed, the eyes were pierced at the corneo-scleral junction and immersed in a tri-aldehyde fixative containing 2.0% glutaraldehyde (Marivac Ltd., Halifax, NS), 1.0% paraformaldehyde (Fisher Scientific Ltd., Toronto, ON) and 1.0% acrolein (Polyscience Inc., Warrington, PA), in sodium cacodylate buffer (0.15M for adults eyes; 0.09M for fetal eyes; 0.10M for neonatal eyes), with 2.0 mM CaCl_2 at pH 7.3. Fixatives were balanced with sucrose to obtain a final osmolarity of 796-808 mOsm for adult eyes, 696-706 mOsm for fetal eyes and 715-725 for neonatal eyes, as determined by a freezing-point depression osmometer (Osmette A, Precision Systems Inc., Sudbury, MA). After 1 hr in fixative at 4°C, the anterior segment of each eye was removed and the posterior pole returned to the fixative for an additional 2 hr.

Following primary fixation, the tissue was cut into small wedge-shaped pieces, so that representative samples from all quadrants of the retina were obtained. These pieces were then placed in a 5.0% buffered-sucrose solution before being osmicated for 1 hr in 1% cacodylate-buffered OsO_4 . The tissue was then stained en block with aqueous uranyl acetate for 1 hr, dehydrated through an ascending acetone series and embedded in TAAB (TAAB Laboratories, Reading, England) low viscosity resin.

Two blocks from each eye, of each animal, were selected at random and oriented such that the photoreceptors were

sectioned parallel to their long axes. Pale-gold sections, approximately 100 nm thick, as judged by the fold technique of Small (1968), were cut using a diamond knife. The sections were collected on large-mesh Formvar-coated grids and stained with saturated aqueous uranyl acetate for 30 min, followed by lead citrate (Reynolds, 1963) for 1 min.

D. Morphological Examination

(i) Three-Dimensional Reconstruction

In order to more readily visualize any changes that might be occurring during the diurnal lighting cycle, three-dimensional reconstructions of selected terminals from representative times in the cycle were undertaken using the same blocks that had been used for the morphometric measurements (see Section D, ii, below). Serial thin sections were cut using a diamond knife and collected on Formvar-coated slotted grids. An average of 45 sections for alpha and paranuclear rods, and 80 sections for cones were needed to traverse the extent of each of these terminals. As with morphometric measurements, only those sections which showed no obvious distortion due to compression or expansion were then photographed on Kodalith 2577 Estar-base 70-mm roll film, at a fixed standard magnification using the monostable mode of the Zeiss EM 10, in order to ensure magnification consistency.

Negative images were projected onto transparent acetate

sheets and the outlines of the terminals, synaptic ribbons, as well as the postsynaptic profiles were colour-coded and traced with felt-tipped pens (Fig. 1a). The acetate tracings were aligned using at least three landmarks other than the terminal that was being reconstructed (Fig. 1b), the profiles were coded, digitized and the data stored in the Zeiss IBAS 1B image analysis computer.

Computer-generated images were then rotated to the desired viewing perspective, a hidden line removal algorithm was run, and the resulting images were subsequently plotted using a Houston Hiplot (DMP-29) digital-plotter. Shading to enhance the three-dimensional perception was added manually.

(ii) Morphometric Measurements

All specimens were coded to prevent any operator prejudice during the various phases of morphometric analysis.

A cascade sampling design (Cruz-Orive and Weibel, 1981) was employed, with a minimum of two animals being sampled at each time. Electron micrographs of synaptic terminals from each sample time and from each of the three photoreceptor types, in adult, fetal and neonatal retinas, were taken at a fixed standard magnification using the monostable mode of the Zeiss EM 10. Initially, serially-sectioned material was used to establish sampling criteria. To ensure that all samples were taken only from the central region (mid-sagittal) of receptor terminals, only those terminals

which contained a synaptic ribbon, were at least 3 to 5 μm in length, and showed invaginations of postsynaptic elements were photographed. That portion of the synaptic terminal extending from the base to a level 3 μm (for rods) and 5 μm (for cones) proximal to the base, were digitized (Fig. 2). These zones were judged to include both the areas of postsynaptic element invagination and vesicle membrane recycling. Accordingly, each synaptic-terminal profile was analysed for size change, by measuring both the terminal area and the perimeter. Shape change was detected by computing a form factor, which in effect measures the amount of infolding of the synaptic terminal membrane (Form Factor = $(4 \pi * \text{AREA}) / (\text{PERIMETER})^2$). Synaptic ribbons within the photoreceptor synaptic terminals were also digitized and their lengths, as well as the absolute number per terminal profile were calculated.

In addition to the above, light micrographs of the outer nuclear layer (ONL), from adult retinas exposed to a diurnal lighting cycle, were taken on 35 mm Plus-X film (Eastman Kodak Co.) using a Zeiss photomicroscope. The nuclei of the paranuclear rods were analysed for nuclear size changes during the 24-hr light:dark cycle, by measuring their perimeter. These additional measurements were made in order to detect any effect that nuclear-size change might have on the synaptic-terminal parameters measured for paranuclear rods, since the measurements of paranuclear rod synaptic terminals necessitated the inclusion of a portion of the

nuclear perimeter (see Fig. 2b).

Statistical analysis of the raw data was accomplished using the BMDP computerized statistical package (BMDP Biomedical Computer Programs, University of California, BMDP-82/CDC Version), using a mixed model of variance and co-variance (BMDP-3V). The results were subsequently plotted against a 24-hr time axis.

(iii) Numerical Density of Synaptic Vesicles

In order to obtain a more complete picture of the synaptic terminal membrane pool, a stereological analysis was run to obtain a statistical estimate of synaptic vesicle packing density (N_V). To effect this three-dimensional calculation, vesicle profiles were photographed at a fixed standard magnification (33,000 X). The images were projected onto the Zeiss IBAS 1B digitizing tablet and were overlaid with a quadrilateral test grid consisting of reference area squares with 0.25 μm sides. All vesicle profiles, and portions of vesicle profiles, contained within alternating grid squares (Gundersen, 1980) were digitized to determine vesicle area, perimeter and maximum diameter. In addition, the section thickness was estimated using the fold technique of Small (1968). Once these parameters were known, IBAS stereological programs were run to estimate the numerical particle (synaptic vesicle) densities (N_V) from

the formula:

$$N_v = \frac{N_a}{(t + 2/3DQ) * AT}$$

N_v = numerical particle density (# particles / μm^3)

N_a = number of particles (per μm^2) in AT

AT = sum of reference areas in μm^2

t = section thickness in μm

DQ = mean of the particle diameters in μm

This IBAS formula is based on an earlier formula ($N_v = N_a \times 1/(D+t)$) used by Abercrombie (1946), but has been modified (IBAS software documentation, 1981) to better estimate numerical particle density, when section thickness is greater than 10% of the particle diameter, and when an area-type (planimetry) analysis is used, as compared to point counting or linear analysis.

Since the vesicle numerical-density (three-dimensional) estimations were ultimately to be used in conjunction with the two-dimensional area and perimeter measurements of synaptic terminals (see Materials and Methods, Section D, ii), these three-dimensional computations had to be converted back to two-dimensional data using the formula $(3\sqrt{N_v})^2$. Since the three-dimensional stereological determinations had taken into consideration both the mean vesicle diameter and the section thickness, these

transformed 2-D data were statistically much more accurate than 2-D data which one might generate directly from a morphometric-type of analysis of the exact same samples.

Once conversions of the numerical densities were completed, values for the number of vesicles per μm^2 and the number of synaptic vesicles per terminal profile were tabulated for each sample time. The raw data were statistically analysed as above, and the results plotted against a 24-hr time axis.

III. RESULTS

A. Qualitative

(i) Light Microscopy - Guinea Pig Retina

(a) Adult

Semi-thin sections were cut through the full width of the retina to ensure that the photoreceptors were being sectioned parallel to their long axes. The adult guinea pig retina (Fig. 3) is similar to other mammalian retinas in that it can be subdivided into ten layers. In Figure 3, beginning with the outermost, or scleral layer, they are: 1) the retinal pigment epithelium (PE), consisting of a single layer of pigmented cuboidal epithelial cells, each with a spherical nucleus near its base and its apical surface in intimate association with the neurosensory retina; 2) the outer and inner segments of photoreceptor cells (rods and cones); 3) the external limiting membrane (ELM), which is not a true membrane, but rather a series of junctional complexes between the retinal glia (Müller cells) and photoreceptor cells; 4) the outer nuclear layer (ONL), composed of the nuclei of the photoreceptors, with cone nuclei being positioned more scleral towards the ELM, and the rod nuclei more vitreal, abutting the next innermost

layer; 5) the outer plexiform layer (OPL), where the photoreceptor synaptic terminals contact dendrites of the bipolar and horizontal cells; 6) the inner nuclear layer (INL), containing the nuclei of the horizontal, bipolar, interplexiform, amacrine and glial (Müller) cells of the retina; 7) the inner plexiform layer (IPL), where the bipolar and amacrine cells synapse with dendrites of the ganglion cells; 8) the ganglion cells layer (GC); the axons of these cells form bundles within the inner retina, giving rise to; 9) the optic nerve fiber layer; and finally, 10) the internal limiting membrane (ILM), which is formed by the apposition of the expanded inner ends of the Müller cells, and, by their basal lamina, separate the retina from the vitreous body of the eye.

(b) Fetal and Neonatal

Fetal and neonatal retinas were also sectioned in a manner similar to the adult tissues. Since the photoreceptor synaptic terminals of both fetal and neonatal retinas were to be compared with adult receptor terminals, it was necessary to establish that the former were fully developed. When the fetal retinas (Fig. 4), which were approximately 62 ± 1 days of gestation, and the neonatal retinas were examined in semi-thin sections, they were observed to: 1) possess all of the layers that had been identified in the adult retina; 2) have discernible photoreceptor outer and inner segments; and 3) have outer

segments sectioned parallel to their long axis. Spira (1975), when studying the development of the guinea pig retina, used the resolution of all ten layers in the retina and the presence of differentiated outer segments as his light microscopic criteria for establishing retinal maturity. The fetal and neonatal retinas used in this study met Spira's (1975) light microscopic criteria for retinal maturity. Electron microscopic examination of these retinas (see Section A, ii, below) was needed to confirm their maturity.

(ii) Electron Microscopy - Synaptic Terminals

The electron microscopic appearance of the three types of photoreceptor synaptic terminals (alpha and paraneuronal rods, and cones) in the guinea pig retina is illustrated in figures 5-7. Both alpha (Fig. 5) and paraneuronal (Fig. 6) rods are associated with a single triad of invaginating neuronal cell processes (*, Fig. 5 and 6), but unlike the alpha rods, paraneuronal rod nuclei (n, Fig. 6) are positioned at the inner border of the ONL, such that they protrude into the synaptic terminals and are in close proximity to invaginating postsynaptic elements (*, Fig. 6). Alternatively, cone synaptic terminals (Fig. 7) possess multiple invaginations from postsynaptic elements (*, Fig. 7) along the whole of their more flattened basal surfaces. Common to all three receptor terminal types are trilaminar, electron-dense structures known as synaptic

ribbons (SRs - arrows, Fig. 5-8). Each SR is positioned in close proximity to a curved, electron-dense structure, the arciform density (open arrow, Fig. 8) which separates the SR from the presynaptic plasmalemma. Some synaptic vesicles (small arrow heads, Fig. 8) are found in close association with the SRs while others are scattered throughout the synaptic terminals of all three photoreceptor cell types.

In addition to the above complement of organelles, each photoreceptor synaptic terminal (both rods and cones) contains an organelle known alternatively as a "synaptic spindle" (Mountford, 1964) or more recently as a "cross-striated filament complex" (Spira and Milman, 1979). These fibrils (arrow heads, Fig. 9-11), when sectioned obliquely, were observed in the cytoplasm of synaptic terminals and can be seen to be composed of thin (6-10 nm) filaments with regular (55-65 nm periodicity) cross-striations (open arrows, Fig. 12). In synaptic terminal profiles from all three photoreceptor cell types that were used for morphometric measurements, these fibril bundles (arrow heads, Fig. 10b) were seen in cross section (approximately 0.1 μ m in diameter) in association with the SR (open arrows, Fig. 10b).

Fetal and neonatal synaptic terminals, when examined at the ultrastructural level, appeared identical to the adult, except that adult terminals are approximately 15% larger. The presence of synaptic vesicles and synaptic ribbons in the photoreceptor synaptic terminals fulfilled the electron

microscopic criteria for functional retinal maturity proposed by Spira (1975). Accordingly, all of the fetal and neonatal retinas used in the present study were judged to be fully developed and functionally mature.

B. Quantitative - Synaptic Terminals

(i) Diurnal Lighting Effects - Adult

(a) Morphometric Measurements

Photoreceptor synaptic terminals from adult guinea pig retinas were examined and photographed at various sample times during a 24-hr diurnal lighting cycle (L:D 12:12); all photographed terminals were then subjected to morphometric analysis in order to evaluate a variety of parameters, including terminal profile area, perimeter, degree of infolding (form factor) and synaptic vesicle density. Variations in these parameters were observed over the diurnal cycle in some or all of the photoreceptor cell types.

In order to determine if photoreceptor synaptic terminal size was changing during the diurnal cycle, terminal profile area was measured. All three photoreceptor cell types demonstrated a significant increase in synaptic terminal sectional area ($p < 0.001$ for alpha rods; $p < 0.04$ for paranuclear rods; $p < 0.008$ for cones) during the light period of the diurnal cycle (Fig. 13). This began with a gradual increase starting 1 hr before lights on ($\bar{x} = 3.1 \mu\text{m}^2$ for alpha rods; $\bar{x} = 2.9 \mu\text{m}^2$ for paranuclear rods; $\bar{x} = 9.6 \mu\text{m}^2$ for cones),

and peaked within 2 hr (1 hr after lights on: $\bar{x}=3.9 \mu\text{m}^2$ for alpha rods; $\bar{x}=3.5 \mu\text{m}^2$ for paranuclear rods; $\bar{x}=11.8 \mu\text{m}^2$ for cones). Over the remainder of the day, terminal profile area gradually declined until 1 hr before lights off, when values were at a similar level to those recorded during the dark period of the cycle (Fig. 13).

Although postsynaptic elements are seen to invaginate into all three synaptic terminal types, in both the light and dark periods of the cycle, qualitative differences appeared to exist in the degree of penetration of these postsynaptic processes, between samples taken in the light and in the dark. In order to quantitate these perceived changes, form-factor measurements (degree of synaptic-terminal membrane infolding) were calculated over the diurnal cycle. A significant reduction ($p<0.001$ for alpha rods; $p<0.004$ for cones) in terminal membrane infolding (postsynaptic processes less deeply invaginated) was indicated when form-factor measurements (Fig. 14a, c) began to increase late in the dark period, in apparent anticipation of lights on; and reached a peak within 4 hrs of the lights coming on ($\bar{x}=0.65$ for alpha rods; $\bar{x}=0.48$ for cones). Conversely, the form factor was also observed to decline towards mid-dark period levels ($\bar{x}=0.35$ for alpha rods; $\bar{x}=0.29$ for cones) as the time for lights out approached, indicating that the terminal plasma membrane was becoming more highly convoluted at this time. As a result, processes of postsynaptic elements appeared both to be more

convoluted, and to penetrate further into the synaptic terminals. Although form-factor measurements obtained from paranuclear rods (Fig. 14b) also appeared to demonstrate a cyclic trend, which was similar to the other two terminal types, clear statistical significance was not obtained ($p=0.065$).

While increases in terminal profile area could be explained by the terminals becoming more rounded through decreased terminal membrane folding (increased form-factor values), terminal profile area could also increase as a result of additions to the terminal plasmalemma surface area. This latter suggestion could be tested by measuring the terminal profile perimeter. When perimeter measurements were computed, significant increases were observed during the mid-light and mid-dark portions of the cycle for both alpha rods ($p<0.003$ - Fig. 15a) and for paranuclear rods ($p<0.001$ - Fig. 15b). From a maximum of $\bar{x}=10.8 \mu\text{m}$ for alpha rods and $\bar{x}=13.7 \mu\text{m}$ for paranuclear rods sampled early in the dark period of the cycle (2330), perimeter values fell, with minimum values being recorded late in the dark period, just prior to lights on (0600: $\bar{x}=8.6 \mu\text{m}$ for alpha rods; $\bar{x}=10.9 \mu\text{m}$ for paranuclear rods) and again early in the dark period, just after lights out (2000: $\bar{x}=8.3 \mu\text{m}$ for alpha rods; $\bar{x}=11.4 \mu\text{m}$ for paranuclear rods). The measurements from cone terminals profiles were equivocal, as they showed a greater perimeter variance during the cycle than did the rods, with the result that no significant change ($p=0.271$) could be

demonstrated during the 12:12 diurnal cycle (Fig. 15c).

In an effort to provide a more complete quantitative assessment of the synaptic-terminal membrane pool, synaptic vesicle size and numerical density were also determined at each sample time. These stereological determinations indicated that mean vesicle diameters were similar in all three synaptic-terminal types ($p=0.235$ for alpha rods; $p=0.520$ for paranuclear rods; $p=0.460$ for cones) and did not vary significantly at any of the sample times during the diurnal lighting cycle (Fig. 16). However, when synaptic vesicle packing density was calculated, a significant increase in the number of vesicles per μm^2 ($p<0.017$ for alpha rods; $p<0.029$ for paranuclear rods; $p<0.011$ for cones) was observed during the light period, for all three receptor cell types (Figs. 17). Further, when these vesicle numerical-density measurements were corrected to reflect synaptic-terminal profile size changes over 24 hr, the results expressed as vesicles per synaptic-terminal profile, became highly significant ($p<0.001$ for alpha rods; $p<0.011$ for paranuclear rods; $p<0.001$ for cones). These data clearly demonstrate increased numbers of vesicles per terminal profile during the light period of the diurnal cycle (Figs. 18).

In addition to the statistical analyses which were run in order to evaluate variations in synaptic terminal morphology for each photoreceptor cell type at each sample time over the complete diurnal cycle, comparisons were also

made of synaptic vesicle density between the three terminal types at each of the sample times. These analyses demonstrated a significant ($p < 0.001$) difference in vesicle numerical density between paranuclear rods and the other two photoreceptor cell types at all sample times; on the average, alpha rods and cones contained 49% more vesicles per μm^2 than did paranuclear rods. There was, however, no such difference between the cones and alpha rods ($p = 0.737$) at any of the times sampled (Fig. 17).

Because of the encroachment of the nucleus into the synaptic terminal region of paranuclear rods, it was necessary to ensure that quantitative evaluations which had been carried out on these synaptic-terminal types had not been influenced by the inclusion of a portion of the nuclear perimeter in the measurements (see Fig. 2b). Accordingly, the perimeters of paranuclear rod nuclei were measured at each sample time during the diurnal cycle and the values subjected to statistical analysis. The calculated p value for paranuclear rod nuclear perimeter measurements ($p = 0.515$) clearly indicates that no statistically significant changes occurred in this parameter during the diurnal cycle.

(b) Three-Dimensional Reconstructions

In order to more readily visualize those changes in photoreceptor synaptic-terminal area, perimeter and shape, that were indicated by morphometric measurements, three-dimensional reconstructions were made for

representative times in light (1100) and dark (0230) periods of the diurnal cycle. The most striking change observed in alpha rod and cone terminals (Figs. 19a, c) was the increased size in the light (Figs. 20a, c) as compared to the dark (Figs. 21a, c). In addition, the alpha rods and cones appeared obviously rounder in the light (Figs. 20a, c), and this had been predicted by the increased form-factor measurements. Differences in paranuclear rods (Fig. 19b) reconstructed from samples taken in the light (Fig. 20b) and dark (Fig. 21b) are not obvious. The subtlety of these changes is, however, reflected in the morphometric values for area ($p < 0.04$) and form factor ($p = 0.065$) differences between these two sample times; the area difference is marginally significant, while the latter falls slightly below statistical significance. Therefore, although changes were often not readily detectable in single sections or even 3-D reconstructions, the statistical analyses of the paranuclear rod data do suggest, however, that differences probably did exist.

(ii) Long-Term Light and Dark Adaptation - Adult

As previous results obtained from eyes sampled at 0600 (late dark) and 0800 (early light) of a normal diurnal lighting cycle have indicated, there was a significant and rapid increase in photoreceptor synaptic terminal area in all three cell types, following the onset of the light portion of the cycle. Whether this "lights-on" event was

being anticipated by these cells (i.e. would terminal area increases have taken place in the absence of lights on) was evaluated by maintaining animals either in the dark or in constant light, for up to 2 wk; samples from both experimental groups were then taken at both 0600 (normal late dark period of diurnally entrained animals) and 0800 (normal early light period of diurnally entrained animals), after 2, 7, and 14 days in these lighting regimes.

The results from long-term light- and dark-adapted retinas indicated that there was no significant differences in synaptic-terminal area values (rods or cones) between the two sample times (0600 and 0800) for either the extended light or extended dark conditions. In addition, contrary to earlier diurnal results, both types of rod terminals exposed to continual darkness became significantly larger ($p < 0.01$ for alpha rods; $p < 0.001$ for paranuclear rods) than their counterparts from the extended light experiment (Figs. 22a, b). Alternatively, cone terminals showed no significant change ($p = 0.10$) between long-term light and dark adaptation (Fig. 22c). However, in spite of the above, when the terminal profile areas from extended light and dark regimes were compared to those values obtained at 0800 in a normal diurnal cycle, the values from extended lighting conditions were significantly ($p < 0.01$) smaller than diurnal values.

(iii) Diurnal Lighting Effects - Fetal

Morphometric determinations carried out on fetal synaptic-terminal profiles were generally unremarkable. Area values did not significantly change in either of the two rod terminal types over the 24-hr sample times ($p=0.075$ for alpha rod; $p=0.174$ for paranuclear rods - Figs. 23a, b). Cone terminal profiles were unchanged as well, except for one significantly increased point ($p<0.01$) occurring shortly after lights on at 0730 (Fig. 23c). The degree of terminal membrane infolding did not appear to change significantly for either paranuclear rods ($p=0.240$) or for cones ($p=0.10$) during the 24-hr cycle (Figs. 24b, c); alpha rods showed only one significantly increased point ($p<0.01$) and this occurred at 1100 in the light period (Fig. 24a). Perimeter measurements for all three synaptic-terminal types showed no significant change ($p=0.089$ for alpha rods; $p=0.075$ for paranuclear rods; $p=0.105$ for cones) during exposure of the pregnant females to a diurnal lighting regime (Fig. 25).

(iv) Diurnal Lighting Effects - Neonatal

In an attempt to determine at what age neonatal retinas would respond in a manner similar to adults retinas when exposed to a diurnal lighting cycle, neonatal animals of 1, 3, 5, and 7 days of age (see Materials and Methods, Section A) were exposed to a 12:12 L:D cycle and sampled 0230 (mid-dark period) and 1330 (mid-light period).

The results from these neonatal retinas (Fig. 26) showed

no statistically significant difference ($p=0.076$ for alpha rods; $p=0.170$ for paranuclear rods; $p=0.546$ for cones) in area values between either 1, 3, 5, or 7 days of age or between the two sample times (0230, 1330).

C. Quantitative - Synaptic Ribbons

(i) Diurnal Lighting Effects - Adults

(a) Three-Dimensional Reconstructions

Reconstructed images of SRs, from both light and dark periods of the diurnal lighting cycle, have demonstrated the complex yet consistent architectonics of these organelles. In both alpha and paranuclear rods, a single horseshoe-shaped ribbon is found in the central basal portion of the terminal, where the postsynaptic elements make contact (Fig. 27). Conversely, cone terminals contain numerous SRs (Fig. 28), and these generally assume a basal location, with the majority concentrated in the central basal region of the terminal where the preponderance of postsynaptic elements invaginate.

Three-dimensional reconstructions of SRs have revealed that these organelles have a finite thickness, as well as width and length. The thickness and width are evident in conventional electron micrographs (Figs. 5-7), where the distance from the first to the third lamina of a SR represents the thickness (Fig. 8). Ribbon width, referred to as length by others (Spadaro et al., 1978; Wagner, 1973; Wagner and Ali, 1977), can be defined as the distance from

the arciform density to the scleral end of each SR profile (Fig. 27a), as viewed in thin sections, and is approximately five times greater than the thickness of the SR. The true length of the SR, can only be appreciated when a ribbon is reconstructed from serial thin sections (Fig. 27b).

In cone terminals, a variety of SR configurations were evident (Fig. 28). These differences are however explained by effecting a series of computer rotations of a single reconstructed SR (Figs. 29 and 30). In figure 29, the SR is positioned such that the viewing perspective is from the first serial section towards the last. The stereo pair of the SR within this terminal (Fig. 29b) shows the SR to be a horseshoe-shaped organelle that is twisted in a number of planes. The middle portion of the SR shows the greatest curvature, while the ends of the SR appear to deviate most from the midline. A side view of this ribbon (Fig. 30) demonstrates its width and length. The stereo pair of this rotation (Fig. 30b) illustrates that the ends of the ribbon are in planes different from the middle portion; it also demonstrates the three-dimensional relationships between ribbon thickness and width.

The reason why these organelles assume such complex conformations became evident when SRs were reconstructed in relation to invaginating postsynaptic elements. The curvature in the middle portion of the SR, which gave the SR its characteristic horseshoe shape, was due to the presence of the bipolar cell process (Fig. 31b). The middle portion

of the SR also conformed to the contours of the processes of horizontal cells which were located laterally (Fig. 31c and d).

By utilizing a representative computer-generated three-dimensional reconstruction of a rod synaptic terminal, together with its SR, it was possible to demonstrate the effect of sectioning angle on both SR 'length' and number (Fig. 32a). Here the ribbon is being viewed from the side, showing its true width and overall length. Three potential sectioning angles (s , s' and s'' , Fig. 32a) are indicated, together with the hypothetical thin-section profiles to be expected from each of these cuts (Figs. 32b-d). If a section were to be taken through the edge of the terminal and ribbon, at an angle slightly oblique to the long axis of the receptor cell (s , Fig. 32a), an artifactual increase in SR numbers could result, due to the curvature at the end of the ribbon (Fig. 32b). Further, a false increase in SR 'length' (Fig. 32c) could also result from a section angle that is tangential to the orientation of the ribbon (s' , Fig. 32a). However, if sections are taken consistently through the longitudinal axis and from the central region of the receptor terminal (s'' , Fig. 32a), the SR will always be cut through its width in its middle portion (Fig. 32d).

(b) Morphometric Measurements

In addition to three-dimensional reconstructions of synaptic ribbons, SR 'length', which is actually ribbon

width, together with the number of ribbons per terminal profile throughout the 24-hr lighting cycle, were determined by morphometric measurements. Synaptic ribbon 'length' was found to have mean values which ranged from 0.24 to 0.36 μm for alpha rods, 0.23 to 0.36 μm for paranuclear rods and 0.29 to 0.36 μm for cones (Figs. 33a, c, e). However, calculated p values (p=0.373 for alpha rods; p=0.270 for paranuclear rods; p=0.285 for cones) indicated that there was no statistically significant change in SR 'length' in any of the three terminal types, during the 12:12 L:D cycle.

The number of SRs per receptor terminal profile was also calculated over the 24-hr cycle (Figs. 33b, d, f). In spite of the larger variation in ribbon numbers in cone terminals (Fig. 33f), the statistical analysis clearly indicated that there was no significant change (p=0.516 for alpha rods; p=0.934 for paranuclear rods; p=0.678 for cones) in the number of SRs per terminal profile, during the light:dark cycle either.

(ii) Long-Term Light and Dark Adaptation - Adult

To test the effect of both long-term light and long-term dark adaptation on synaptic ribbon length and numbers, synaptic ribbons from photoreceptor synaptic terminals of retinas that had been sampled after 2, 7, and 14 days in continuous light or continuous dark were measured. The mean SR 'length' for extended light regime samples ranged from 0.16 to 0.49 μm for alpha rods, 0.21 to 0.27 μm for

paranuclear rods and 0.27 to 0.31 μm for cones. The mean values for SR 'length' in synaptic terminals exposed to continuous darkness ranged from 0.20 to 0.27 μm for alpha rods, 0.24 to 0.30 μm for paranuclear rods and from 0.27 to 0.33 μm for cones.

When p values were calculated for SR 'length' (Fig. 34a, c, e) they showed that there was no statistically significant difference ($p=0.544$ for alpha rods; $p=0.183$ for paranuclear rods; $p=0.764$ for cones) between either long-term light or dark adaptation; the two sample times (0600 and 0800); or among the number of days in a given lighting condition (2, 7, 14 days). Similarly, when p values were calculated for the number of SRs per terminal profile, it was clear that no significant change ($p=0.634$ for alpha rods; $p=0.722$ for paranuclear rods; $p=0.120$ for cones) had occurred between any of the experimental conditions (sample times, number of days in a lighting condition or type of lighting condition - Fig. 34b, d, f).

(iii) Diurnal Lighting Effects - Fetal

Synaptic ribbon 'lengths', when calculated for fetal synaptic terminals, were found to have mean values which ranged from 0.28 to 0.39 μm for alpha rods, 0.34 to 0.45 μm for paranuclear rods and from 0.31 to 0.38 μm for cones. When analysed, no statistically significant changes in SR 'length' was evident (Fig. 35a, c, e) in any of the synaptic-terminal types during the 24-hr cycle, as indicated

by calculated p values of 0.717 for alpha rods, 0.210 for paranuclear rods and 0.755 for cones. Similar to adult synaptic terminals, there was no statistically significant change ($p=0.170$ for alpha rods; $p=0.827$ for paranuclear rods; $p=0.183$ for cones) in the number of synaptic ribbons per fetal synaptic terminal during this diurnal cycle either (Fig. 35b, d, f).

(iv) Diurnal Lighting Effects - Neonatal

Neonatal animals were sampled at 0230 in the dark period of a diurnal lighting cycle, and at 1330, in the light period of the cycle. Neonatal SR 'length' values ranged from 0.19 to 0.22 μm in alpha rods; 0.21 to 0.24 μm in paranuclear rods; and from 0.22 to 0.26 μm in cones. Calculated p values of 0.150 for alpha rods, 0.282 for paranuclear rods and 0.524 for cones indicated that there was no significant change (Fig. 36a, c, e) between either the two sample times (0230, 1330), or between the four sample ages (1, 3, 5, 7 days).

Morphometric measurements on the number of SRs per terminal (Fig. 36b, d, f) indicated that, just as for both adult and fetal terminals, no statistically significant differences existed ($p=0.587$ for alpha rods; $p=0.550$ for paranuclear rods; $p=0.427$ for cones) between the sample times, or between the four different age groups.

FIGURE 1

a. Photograph of colour-coded synaptic terminal tracings on a transparent acetate sheet. This tracing, from the central region of a cone terminal (serial section number 41), shows the terminal that is being reconstructed (open arrows) as well as other terminals (*) that are present on the electron micrograph negative. The crosses (arrow heads) are added to serve as reference points when the tracings are digitized on the IBAS 1B.

b. Photograph of a series of aligned acetate tracings (serial sections numbers 41-47) of the cone terminal illustrated in figure 1a. The acetate tracings are aligned using at least three landmarks (*) other than the terminal that is being reconstructed (open arrows). After a tracing is added to the aligned series, the reference points (arrow heads) are drawn in to indicate the sheet's relative position in the series so that this position can be maintained when the tracing is digitized on the IBAS 1B.



41



FIGURE 2

- a. Alpha Rod
- b. Paranuclear Rod
- c. Cone

Schematic drawing of the different types of photoreceptor synaptic terminals found in the guinea pig retina. The narrow lines (*) indicate the template used for the measurement of the rod and cone terminals. The area, perimeter and the amount of infolding were calculated from tracings that followed the outline indicated by the thick line (open arrows).

n=nucleus

Bar = 1.0 μ m

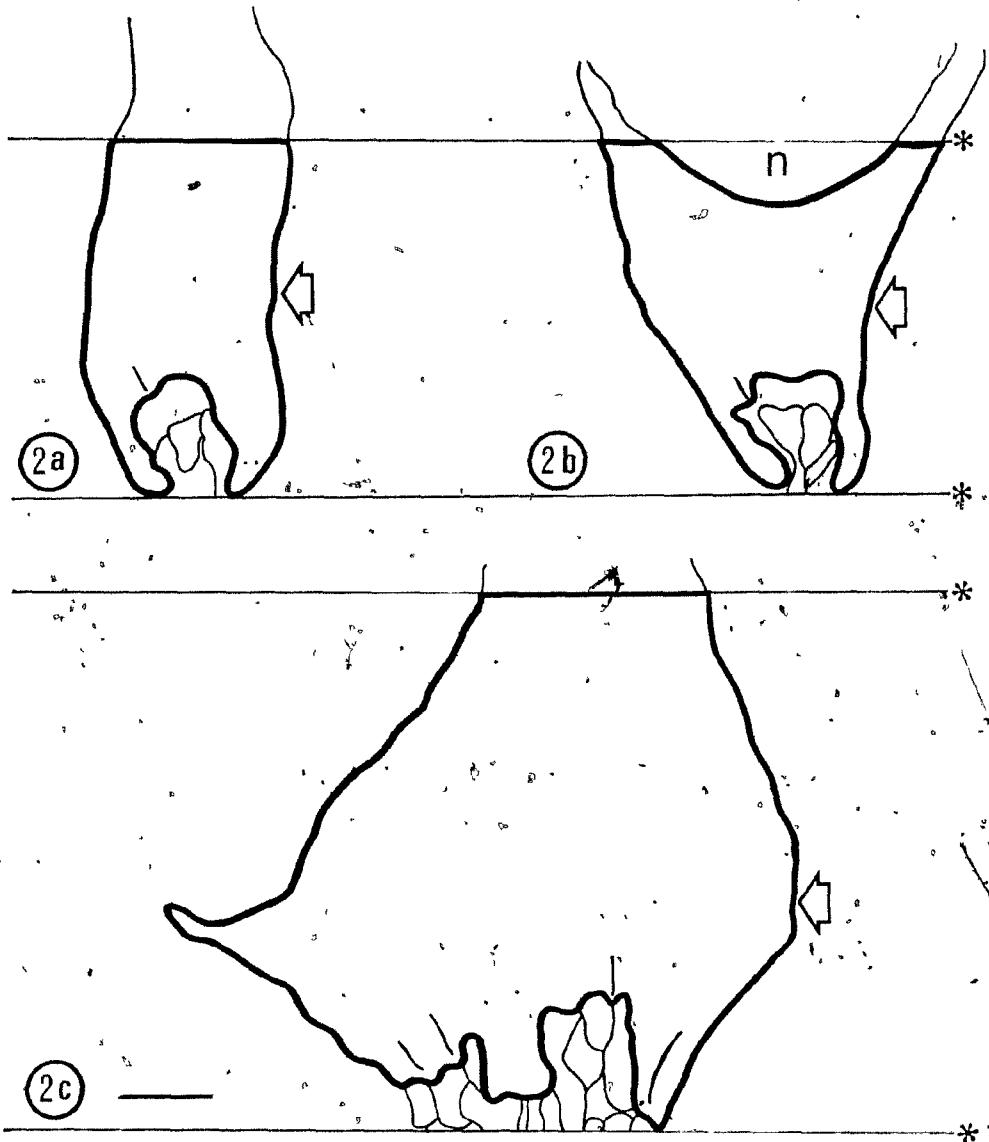
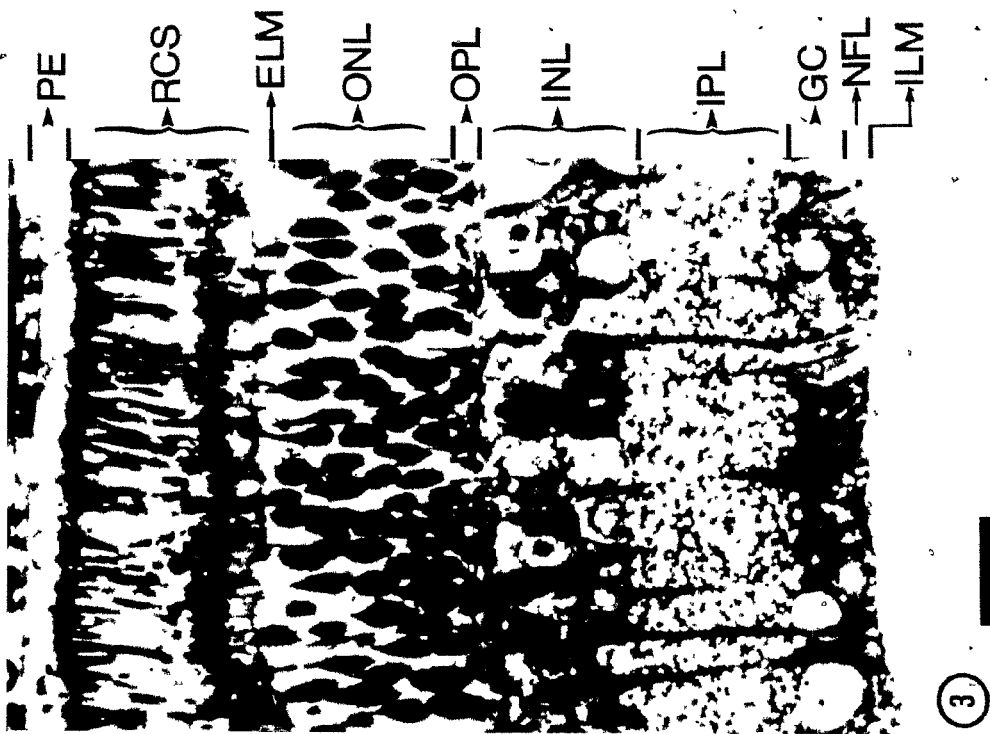
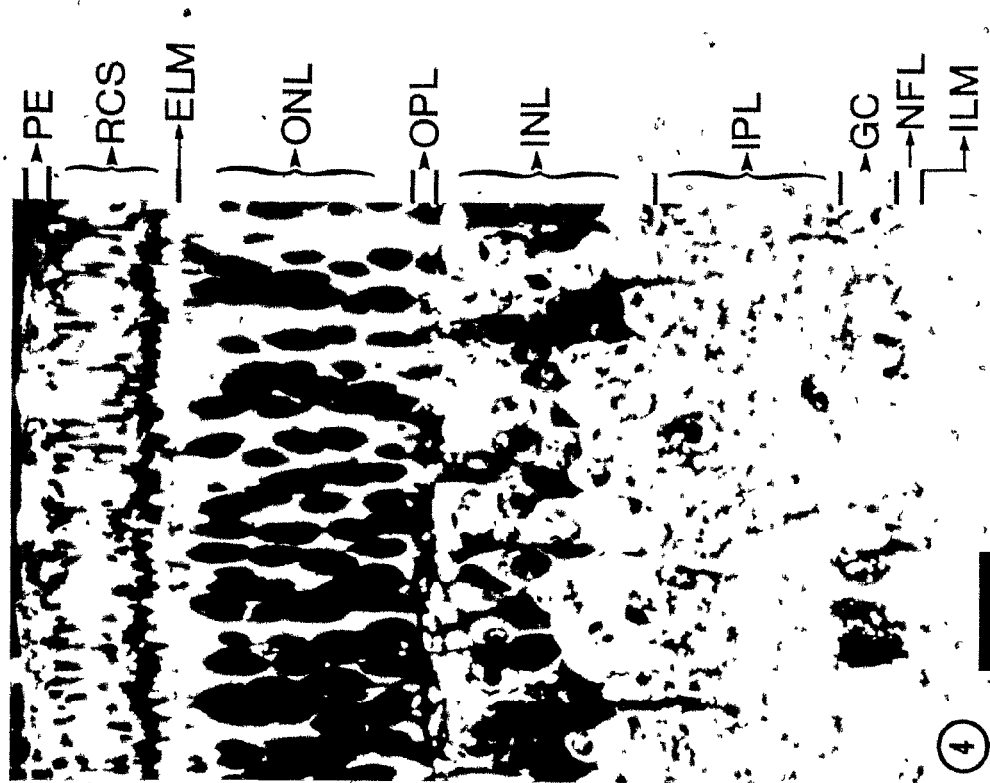


FIGURE 3 (Adult), 4 (Fetal)

Light micrographs of the full thickness of the adult (Fig. 3) and fetal (Fig. 4) guinea pig retinas. Beginning at the scleral side, both retinas exhibit ten histological layers which include; 1) the pigment epithelium (PE); 2) rod and cone outer and inner segments (RCS); 3) the external limiting membrane (ELM); 4) the outer nuclear layer (ONL); 5) outer plexiform layer (OPL); 6) inner nuclear layer (INL); 7) inner plexiform layer (IPL); 8) ganglion cell layer; 9) optic nerve fiber layer (NFL); and finally 10) the inner limiting membrane (ILM). At 62 ± 1 days of gestation, the fetal retina (Fig. 4) is thinner than the adult retina (Fig. 3), but is considered to be functionally mature based on the criteria of Spira (1975).

Bar = 5.0 μ m



FIGURES 5 (Alpha Rod), 6 (Paranuclear Rod), 7 (Cone).

Electron micrographs of mid-sagittal sections through the three types of photoreceptor synaptic terminals found in adult, fetal and neonatal guinea pig retinas. Although the terminals illustrated here are from an adult retina, they show the same characteristics as the photoreceptor synaptic terminals of fetal and neonatal retinas, except that they are approximately 15 % larger. All three terminal types show invaginations of postsynaptic elements (*) in close relationship to the synaptic ribbons (SRs-arrow heads). Both the alpha and paranuclear rods contain a single SR profile and generally have similar morphological characteristics, except that the nucleus (n) of the paranuclear rod is positioned within the inner portion of the outer nuclear layer, immediately adjacent to the synaptic terminal. The larger cone terminals have numerous SRs, each of which is associated with one group of invaginating postsynaptic elements.

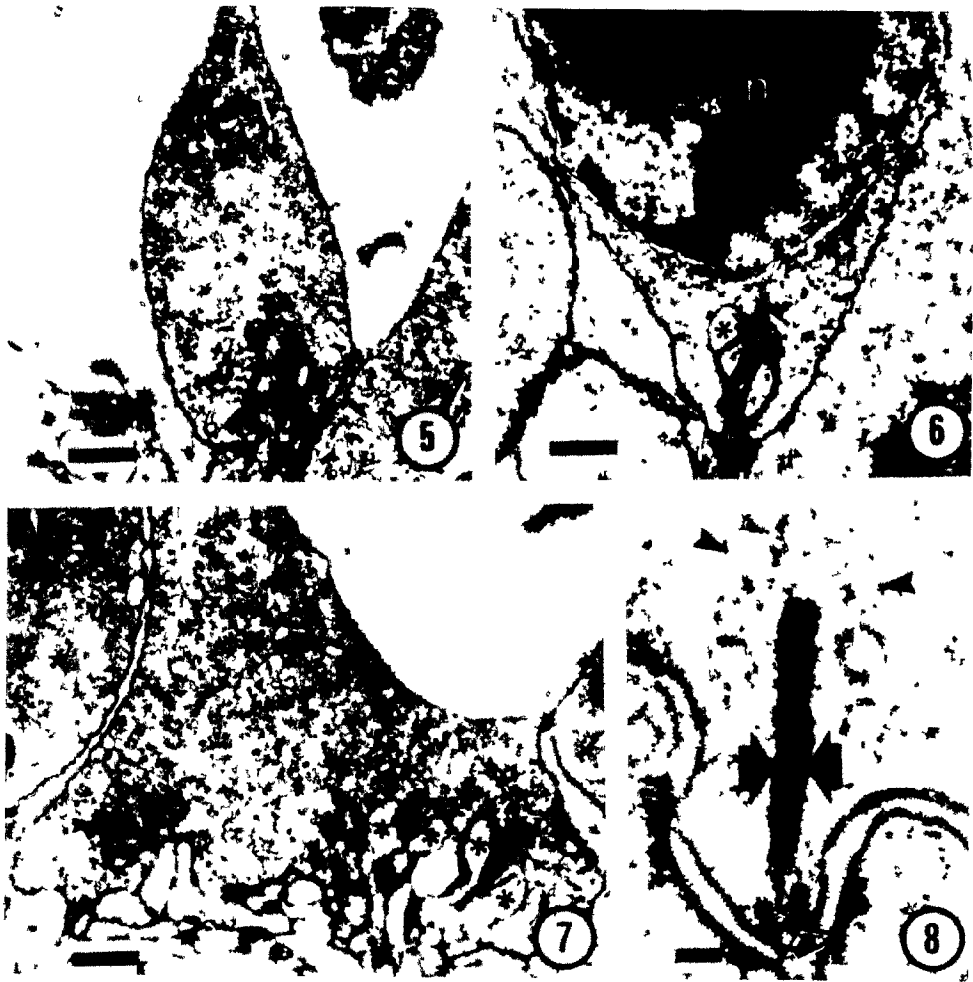
Bar = 0.5 μ m

FIGURE 8:

Electron micrograph of a synaptic ribbon (SR) from a cone terminal showing the trilaminar appearance evident in

thin sections. The dimension indicated by the large arrows represents the thickness of the ribbon. The relationships of the synaptic vesicles (arrow heads), which are also distributed throughout the synaptic terminal, and the arciform density (open arrow) to the SR are also shown.

Bar = 50 nm



FIGURES 9 (Alpha Rod), 10 (Paranuclear Rod), 11 (Cone)

Transmission electron micrographs illustrating the cross-striated fibril (arrow heads) that was noted in all three photoreceptor synaptic-terminal types found in the guinea pig retina. When sectioned obliquely, these fibrils (arrow heads, Fig. 9, 10a, 11) were seen running through the cytoplasm of the synaptic terminals. In longitudinal sections from the central region of all three photoreceptor synaptic-terminal types, a cross section of the fibril (here illustrated in a paranuclear rod - arrow heads, Fig. 10b) was seen associated with the synaptic ribbon (open arrows, Fig. 10b).

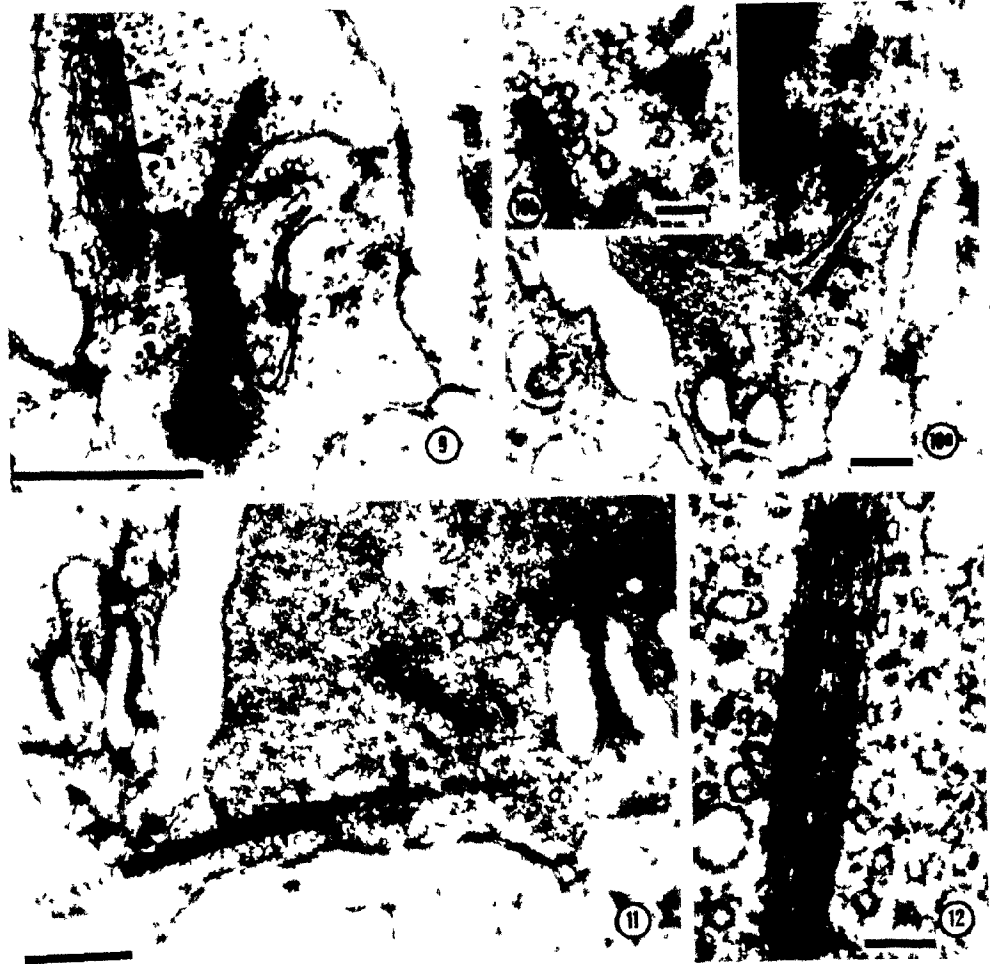
Figures 9, 10a, 11 - Bar = 0.5 μ m

Figure 10b - Bar = 0.1 μ m

FIGURE 12

Transmission electron micrograph of a cross-striated fibril from the synaptic terminal of a cone. The higher magnification of this micrograph illustrates both the thin filaments (6-10 nm) that make up the bulk of the fibril, as well as the regularly spaced (55-65 nm) cross-striations (open arrows).

Bar = 0.1 μ m



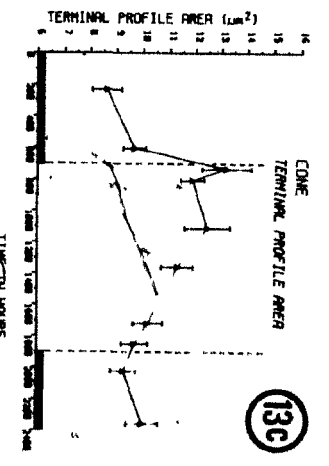
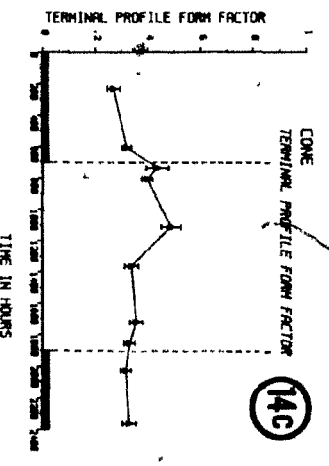
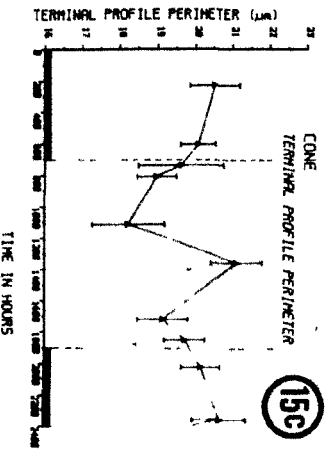
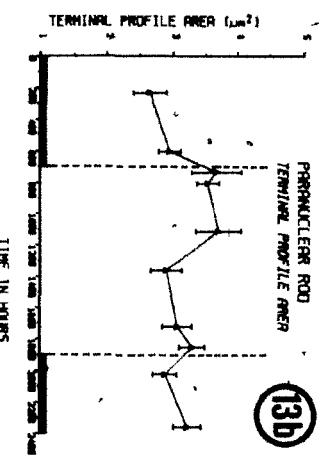
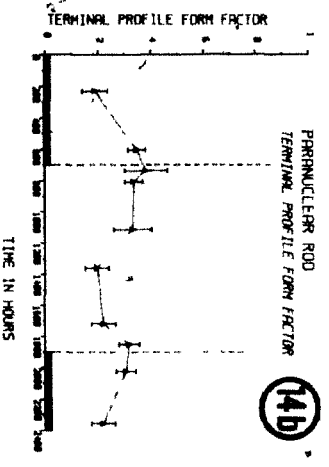
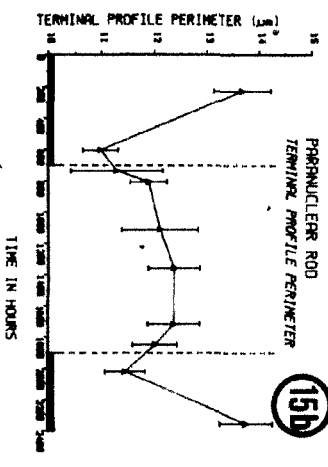
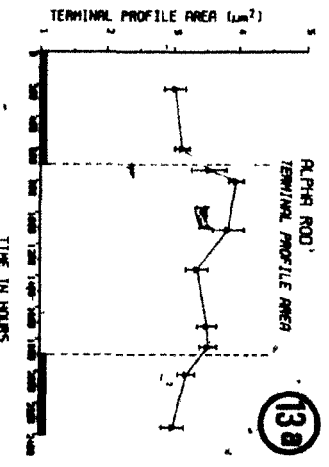
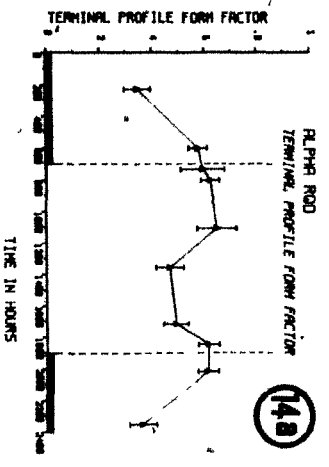
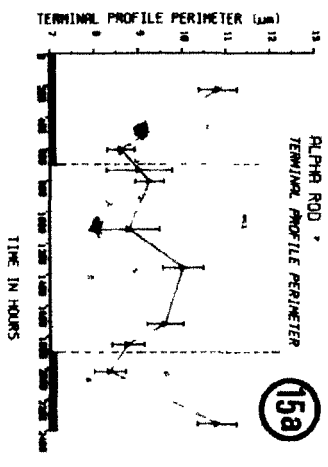
FIGURES 13, 14, 15

These figures illustrate the changes in area, perimeter and form factor that occurred in guinea pig photoreceptor synaptic terminals at 10 sample times over a 24-hr cycle; a = alpha rod, b = paranuclear rod, c = cone; all data points represent mean sample values \pm S.E.M.

Figure 13, shows the variation in terminal profile area with time, where all three photoreceptor cell types demonstrated a significant increase ($p < 0.001$ for alpha rods; $p < 0.040$ for paranuclear rods; $p < 0.008$ for cones) in synaptic-terminal sectional area during the light period of a diurnal cycle.

Figure 14, shows the relationship between the terminal profile form factor (degree of infolding) and sample times. Form-factor measurements for alpha rods ($p < 0.001$) and for cones ($p < 0.004$) showed a significant increase (terminals become more rounded) during the light period. Although paranuclear rod form-factor measurements also appeared to demonstrate a similar cyclic trend, clear statistical significance was not obtained ($p = 0.065$).

Figure 15, shows the relationship between the terminal profile perimeter and sample times. Significant increases occurred during both the mid-light and mid-dark periods of the cycle for both the alpha rods ($p < 0.003$) and paranuclear rods ($p < 0.001$). Measurements from cone terminals were equivocal, as they showed a higher degree of variance than did the rods, with the result that no significant change ($p = 0.271$) could be distinguished.



FIGURES 16, 17, 18.

These figures illustrate changes in vesicle density that occur in guinea pig photoreceptor synaptic terminals, at 10 sample times over a 24-hr period; a = alpha rod, b = paranuclear rod, c = cone; all data points represent mean sample values \pm S.E.M.

Figure 16, shows the relationship between the mean synaptic vesicle diameter and sample times. Stereological determinations indicated that the mean vesicle diameters were similar in all three synaptic-terminal types and did not vary significantly ($p=0.235$ for alpha rods; $p=0.520$ for paranuclear rods; $p=0.460$ for cones) during the diurnal cycle.

Figure 17, shows the relationship between the number of vesicles per μm^2 and sample times. All three receptor cell types showed significant increases ($p<0.017$ for alpha rods; $p<0.029$ for paranuclear rods; $p<0.011$ for cones) in vesicle density during the light period.

Figure 18, shows the relationship between the number of vesicles per terminal profile and sample times, when vesicle numerical density measurements were corrected for terminal

profile size changes over 24 hr. The results showed that there were significantly more vesicles per terminal profile during the light period ($p < 0.001$ for alpha rods; $p < 0.011$ for paranuclear rods; $p < 0.001$ for cones).

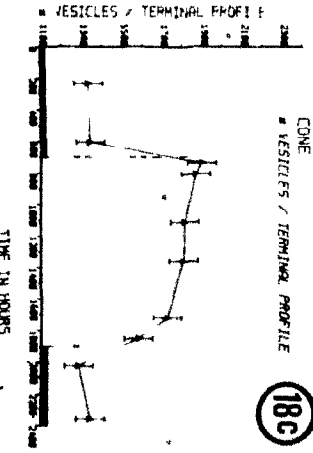
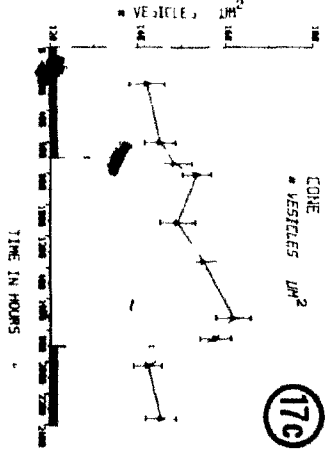
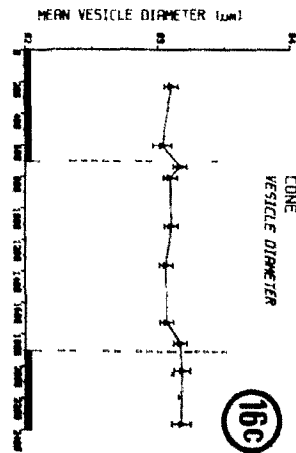
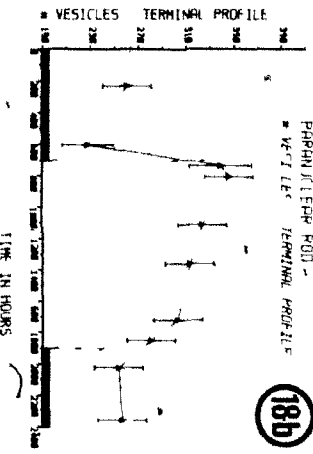
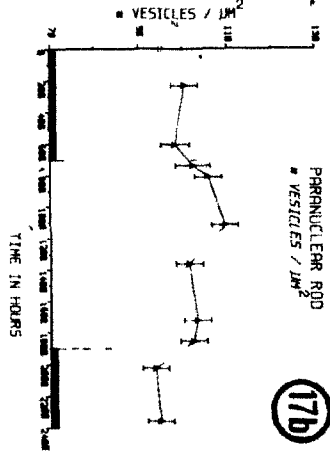
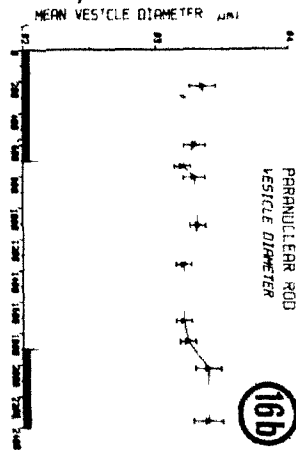
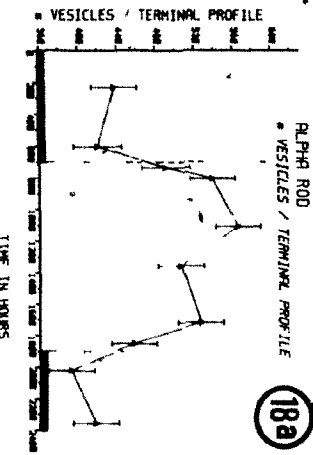
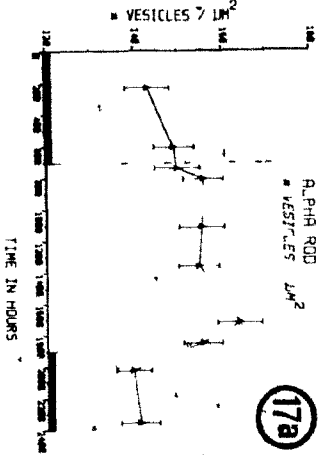
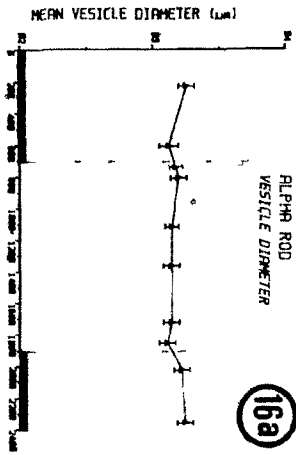


FIGURE 19.

Transmission electron micrographs of mid-sagittal sections through the three types of photoreceptor synaptic terminals found in the guinea pig retina. These terminals, sampled during the light period of a diurnal cycle, all show invaginations of postsynaptic elements (*) in close relationship to the synaptic ribbon (SR) (arrow heads). Alpha (a) and parancular rods (b) contain a single SR associated with a single group of invaginating postsynaptic elements, while the cone (c) contains numerous SRs, each associated with a group of invaginating postsynaptic elements.

Bar = 0.5 μ m.

Figures 20 and 21.

Three-dimensional reconstructions of photoreceptor synaptic terminals beginning in a mid-sagittal plane; these reconstructions were made from two representative times, 1100 in the light period (Fig. 20) and 0230 in the dark period (Fig. 21) of a diurnal cycle. Alpha rod (a) and cone (c) terminals in Fig. 20 appear larger and rounder than their counterparts sampled in the dark period (Fig. 21).

The subtlety of these changes in paranuclear rods (b) between sample times in the light and dark, is reflected in the morphometric values for area ($p < 0.04$) and form factor ($p = 0.065$). Since all rotational conditions for each pair (light vs dark sample times) of reconstructions are equal, any observable differences between figures 20 and 21 can not be attributed to rotational distortions.

Bar = 1.0 μm



20a



21a

20b



21b

20c



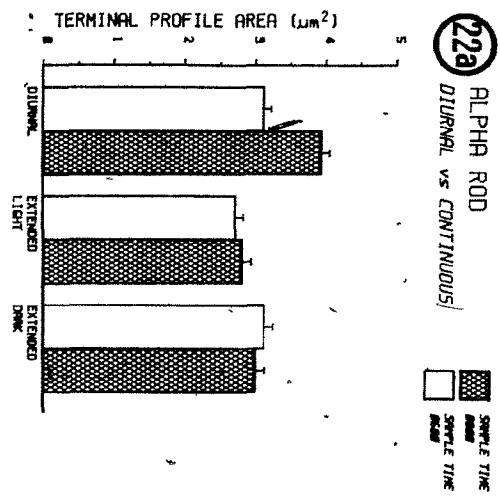
21c



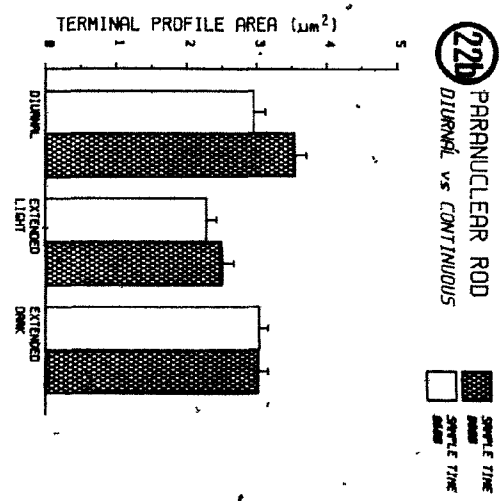
FIGURE 22.

Histograms comparing terminal profile area values obtained in diurnal and long-term light or dark conditions. The mean values \pm S.E.M. area are illustrated. Since no significant differences existed between values for 2, 7 or 14 days in extended lighting conditions, the bars on the graphs represent the results of pooled sample values. No differences were observed in any of the three terminal types, between the two sample times (0600 and 0800) in either the extended light or extended dark regimes. Both alpha (a) and paranuclear (b) rod terminals exposed to continual darkness were significantly larger ($p < 0.01$ for alpha rods; $p < 0.001$ for paranuclear rods) than their counterparts from the extended light regime. Cone (c) terminals showed no significant change ($p = 0.10$) between long-term light and dark adaptation. None of the terminals from the extended conditions approached the values obtained under L:D conditions and sampled at 0800 ($p < 0.01$) (see figure 13).

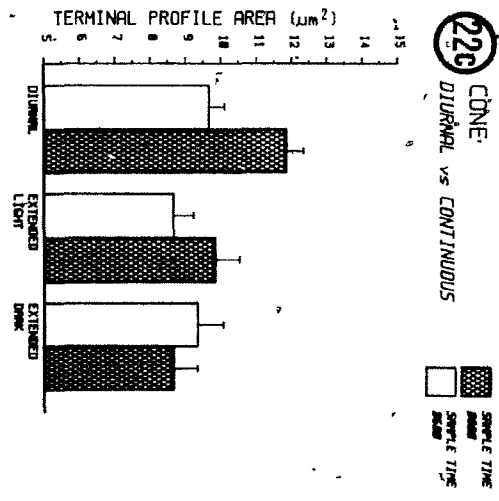
22a ALPHA ROD
DIURNAL VS CONTINUOUS



22b PARANUCLEAR ROD
DIURNAL VS CONTINUOUS



22c CONE
DIURNAL VS CONTINUOUS



FIGURES 23, 24, 25.

These figures illustrate the relationship between fetal photoreceptor synaptic terminal profile area (Fig. 23), form factor (Fig. 24) and perimeter (Fig. 25) at 10 representative sample times during a diurnal lighting cycle. Alpha rod (a) and paranuclear rod (b) area measurements showed no significant change ($p=0.075$ for alpha rods; $p=0.174$ for paranuclear rods), while cone (c) terminal profile area measurements had only one significantly increased ($p<0.01$) point, at 0730. The degree of terminal membrane infolding (Fig. 24) did not change significantly for either paranuclear rods (b) ($p=0.240$) or for cones (c) ($p=0.10$) over the 24-hr cycle. Alpha rods (a) showed only one significantly increased point (amount of infolding increased - $p<0.01$) at 1100 in the light period. The perimeter measurements (Fig. 25) for all three terminal types did not change significantly ($p=0.089$ for alpha rods; $p=0.075$ for paranuclear rods; $p=0.105$ for cones) during the L:D cycle.

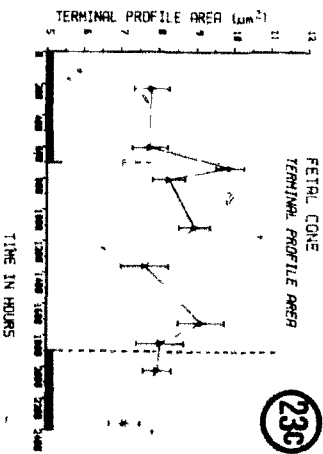
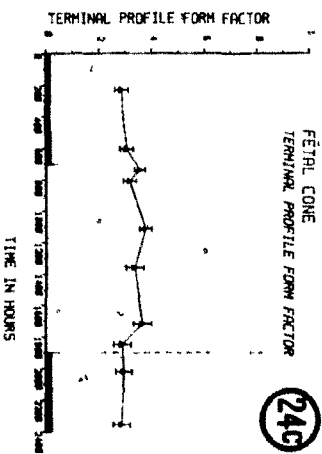
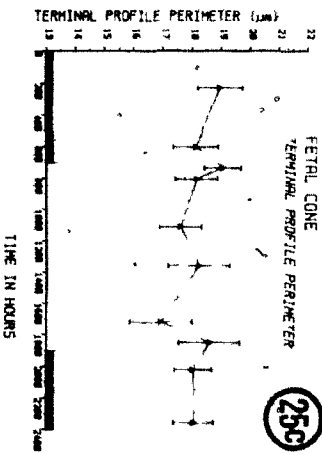
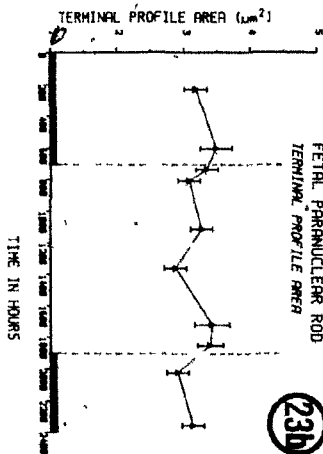
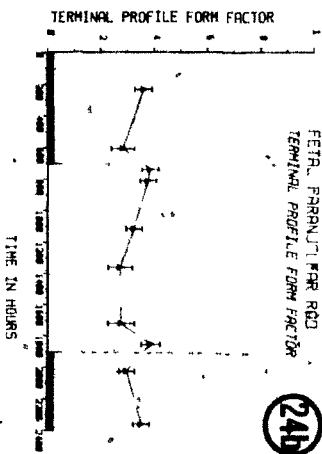
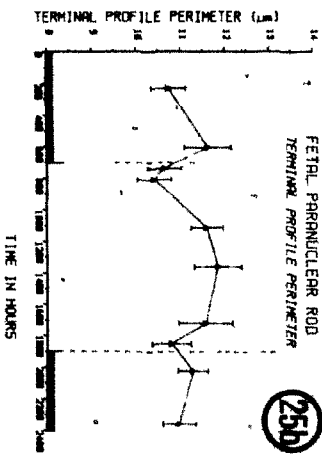
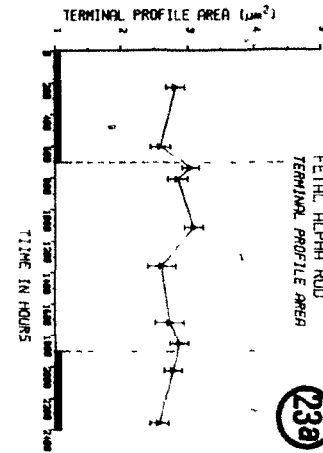
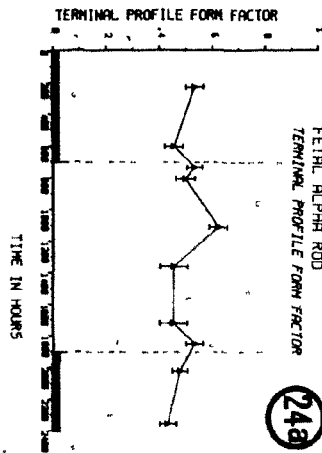
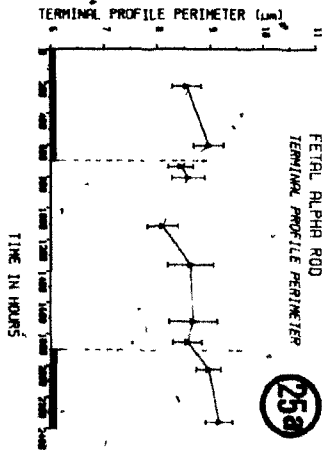
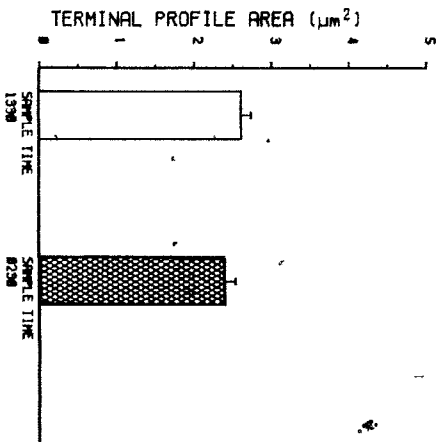


FIGURE 26

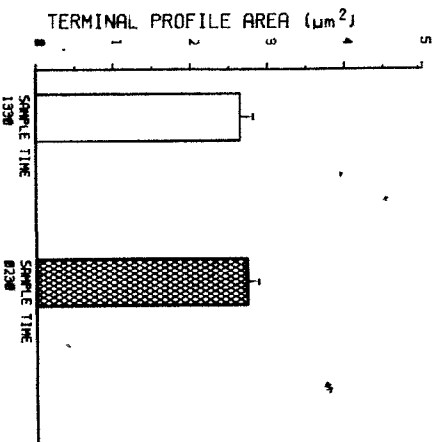
- a. Alpha Rod
- b. Paranuclear Rod
- c. Cone

Histograms comparing the terminal profile area values of neonatal guinea pigs obtained at two sample times (1330 - light) (0230 - dark) in a diurnal cycle. The mean values \pm S.E.M. are illustrated. Statistical analyses revealed that there was no significant differences ($p=0.076$ for alpha rods; $p=0.170$ for paranuclear rods; $p=0.546$ for cones) in area values between either 1, 3, 5, or 7 days of age, or between the two sample times. Since no significant differences existed between values for 1, 3, 5 or 7 days of age, the bars on the graphs represent the results of pooled sample values.

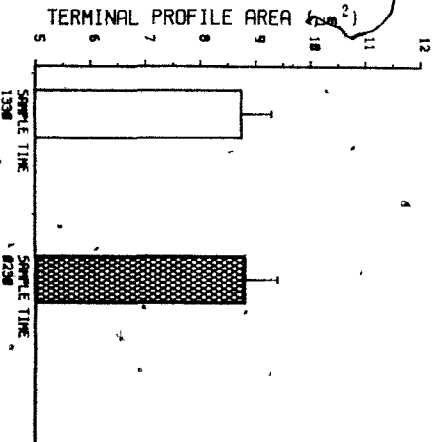
26a NEONATAL ALPHA ROD
TERMINAL PROFILE AREA



26b NEONATAL PARANUCLEAR ROD
TERMINAL PROFILE AREA



26c NEONATAL CONE
TERMINAL PROFILE AREA



FIGURES 27 (Alpha Rod), 28 (Cone).

a. A partial 3-D reconstruction, beginning near the mid-sagittal region of the synaptic terminal. The synaptic ribbon (SR) is shown in sectional profile, as a plate-like structure, in close apposition to the invaginations of the postsynaptic elements.

b. A 3-D reconstruction of the synaptic ribbon(s) as it (they) appear when isolated from the terminal. In figure 27b, the relationship between ribbon width (w) and length (l) is illustrated.

c. A 3-D reconstruction of the whole synaptic terminal; the exact position and shape of the SR(s) within the terminal is (are) also illustrated.

Bar = 1 μ m



27c



28c



27b

28b



27a

28a



FIGURE 29.

a. Three-dimensional reconstruction of an alpha rod synaptic terminal showing the position and apparent shape of the synaptic ribbon (SR), when the terminal is rotated such that it is viewed from the first serial section towards the last.

b. A stereo pair of the reconstructed SR from the terminal in figure 29a above.

Bar = 0.5 μ m

FIGURE 30.

a. Three-dimensional reconstruction of the same synaptic terminal viewed in Figure 29a; the terminal has been rotated through approximately 45° along its long axis.

b. A stereo pair of the reconstructed SR from figure 30a.

Bar = 0.5 μ m



29a



30a



29b



30b

FIGURE 31.

a. Schematic representation of a mid-sagittal slice through an alpha rod* synaptic terminal, showing postsynaptic elements of a horizontal cell (h), bipolar cell (b) and a second horizontal cell (hl).

b,c,d. Computer-generated 3-D reconstructions of the synaptic ribbon (SR) from an alpha rod, together with postsynaptic cell processes.

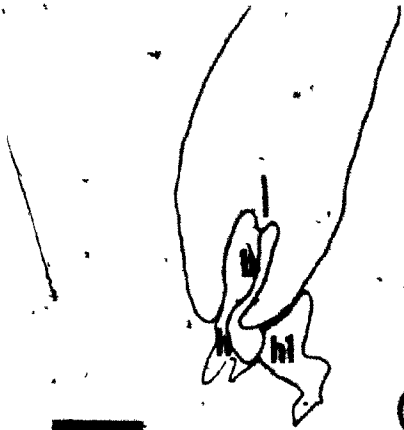
b.- Bipolar cell (b)

c.- Horizontal cell (hl)

d.- Horizontal cell (h)

* reconstruction of synaptic terminals from paranuclear rods and cones show similar relationships between the SR and postsynaptic elements.

Bar = 0.5 μ m



31a



31b



31c



31d

FIGURE 32.

Three-dimensional reconstruction of a synaptic ribbon (SR) within an alpha rod synaptic terminal. This reconstruction demonstrates that, if samples were to be taken from the edge of the terminal (s; 32b), there could be an apparent greater number of ribbons, or greater ribbon 'length' (s'; 32c), as a result of tangential ribbon sections, as compared to a midline sagittal section (s''; 32d) which allows for a consistent measurement of ribbon width ('length').

Bar = 0.5 μ m

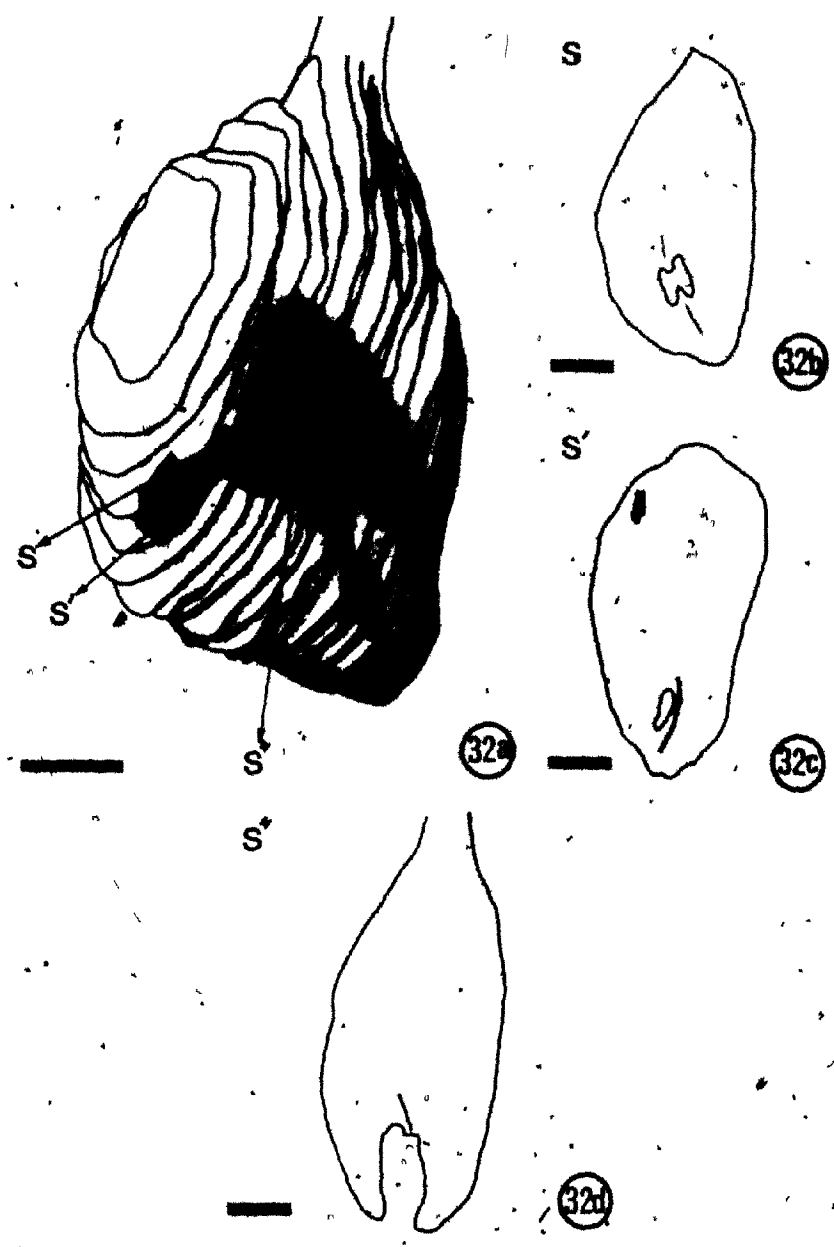


FIGURE 33.

Graphs showing the relationship between synaptic ribbon (SR) length and sample time (a,c,e) and between the number of SRs per terminal profile and the time in the cycle (b,d,f). The mean values \pm S.E.M. for the data collected at the various times throughout the L:D cycle, are illustrated. Calculated p values for SR length (p=0.373 for alpha rods; p=0.270 for paranuclear rods; p=0.516 for cones) and for the number of SR per terminal profile (p=0.516 for alpha rods; p=0.934 for paranuclear rods; p=0.678 for cones) indicated that no significant change occurred in these parameters during the 24-hr cycle.

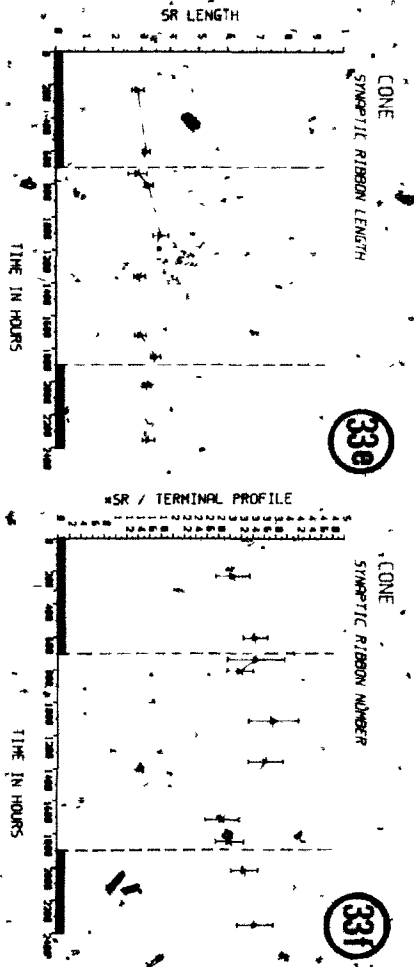
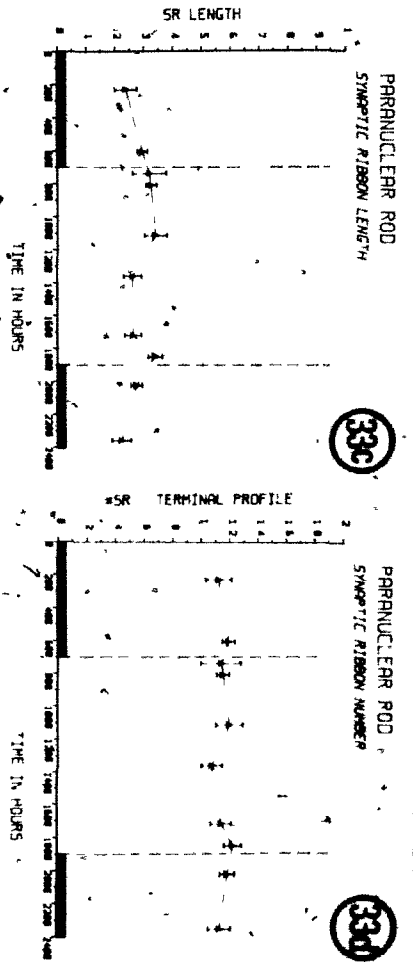
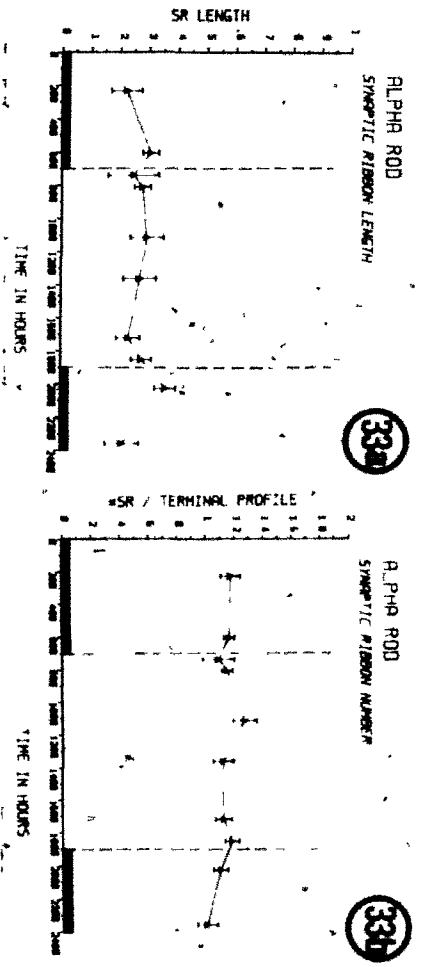
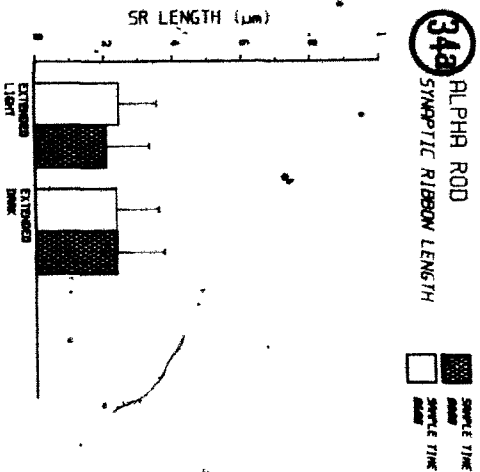


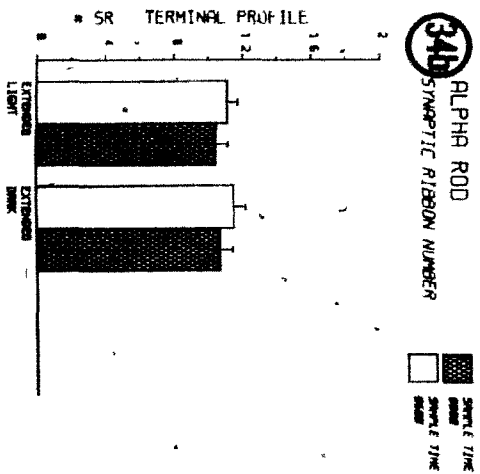
FIGURE 34

Histograms showing the relationship between synaptic ribbon (SR) length and sample time (a, c, e), and between the number of SRs per terminal profile and sample time (b, d, f) in adult animals exposed to extended light (L:L) and extended dark (D:D) conditions. The mean values \pm S.E.M. are illustrated. Calculated p values for SR length (p=0.544 for alpha rods; p=0.183 for paranuclear rods; p=0.764 for cones) indicated that there were no statistically significant differences between the two sample times (0600, 0800), the number of days in a given lighting condition (2, 7, 14 days), or between continuous light (L:L) or continuous dark (D:D) regimes. Since no significant differences existed between values for 2, 7 or 14 days in extended lighting conditions, the bars on the graphs represent the results of pooled sample values. The p values calculated for the number of SRs per terminal profile (p=0.634 for alpha rods; p=0.722 for paranuclear rods; p=0.120 for cones) also indicated that significant changes had not occurred in this parameter between any of the experimental conditions (sample time, number of days in lighting regime, or type of lighting condition).

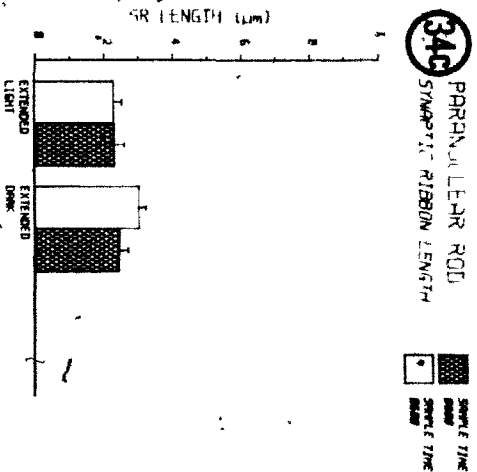
34a ALPHA ROD
SYNAPTIC RIBBON LENGTH



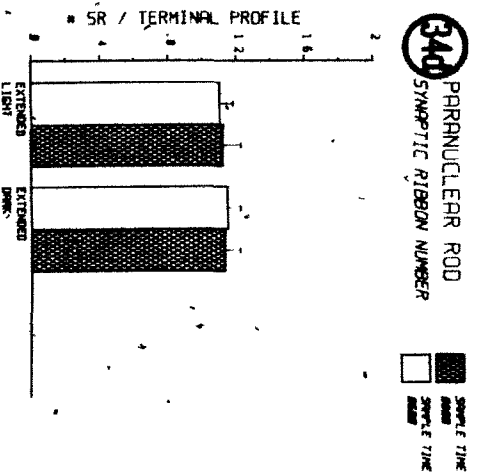
34b ALPHA ROD
SYNAPTIC RIBBON NUMBER



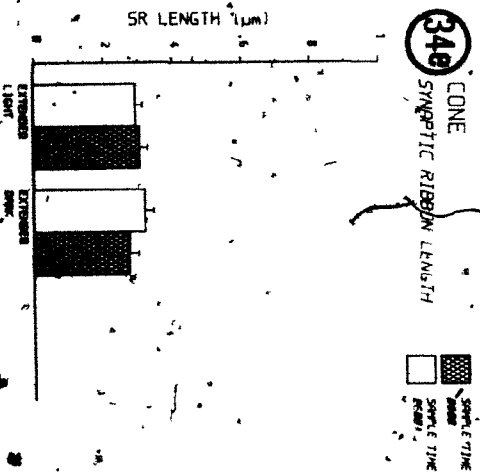
34c PARANUCLEAR ROD
SYNAPTIC RIBBON LENGTH



34d PARANUCLEAR ROD
SYNAPTIC RIBBON NUMBER



34e CONE
SYNAPTIC RIBBON LENGTH



34f CONE
SYNAPTIC RIBBON NUMBER

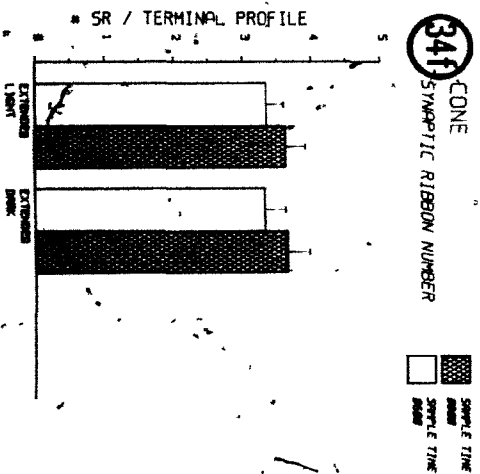
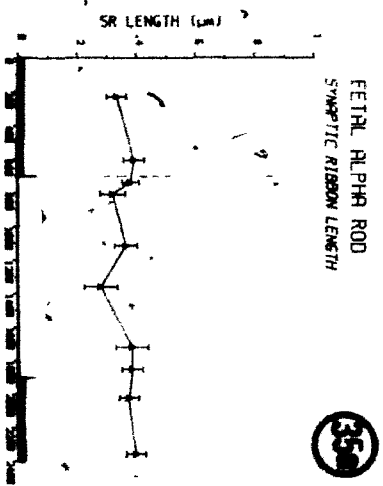
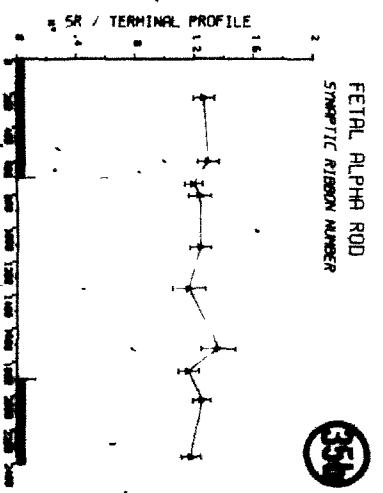


FIGURE 35

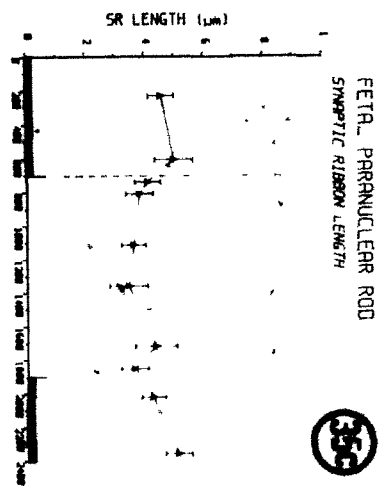
Graphs showing the relationship between synaptic ribbon (SR) length and sample time (a, c, e), and between the number of SRs per terminal profile and the time in the lighting cycle (b, d, f). The mean values \pm S.E.M. are illustrated for the fetal data collected at various times throughout the L:D cycle. Calculated p values for SR length ($p=0.717$ for alpha rods; $p=0.210$ for paranuclear rods; $p=0.755$ for cones) and for the number of SRs per terminal profile ($p=0.170$ for alpha rods; $p=0.827$ for paranuclear rods; $p=0.183$ for cones) indicated that statistically significant changes had not occurred in these parameters during the 24-hr cycle.



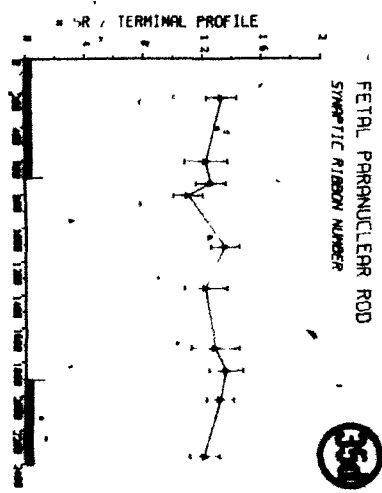
354



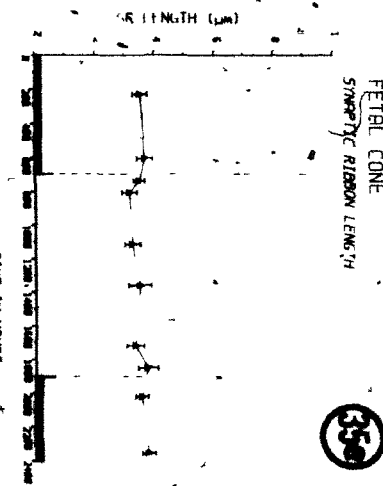
354



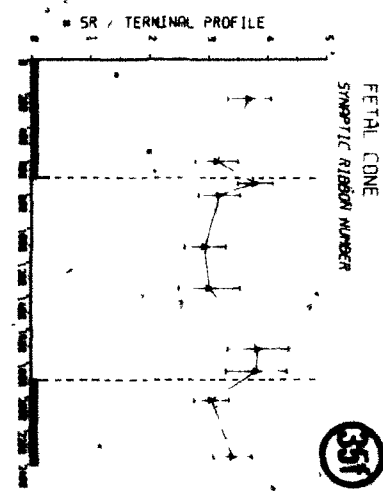
355



355



356

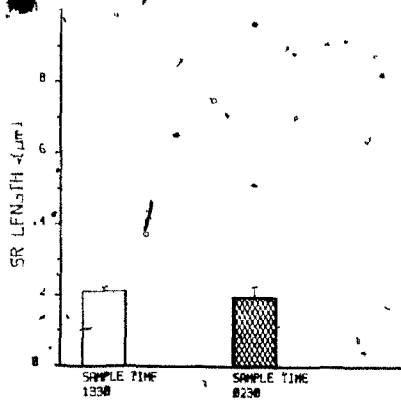


356

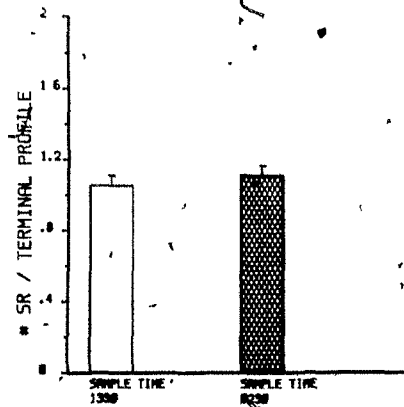
FIGURE 36

Histograms showing the relationship between synaptic ribbon (SR) length and sample time (a, c, e), and between the number of SRs per terminal profile and sample time (b, d, f), in neonatal animals exposed to a diurnal cycle. The mean values \pm S.E.M. are illustrated. Calculated p values for SR length ($p=0.150$ for alpha rods; $p=0.282$ for paranuclear rods; $p=0.524$ for cones) indicated that there was no statistically significant difference between the two sample times (1330, 0230) or between the four neonatal ages (1, 3, 5, 7 days). Since no significant differences existed between values for 1, 3, 5 or 7 days of age, the bars on the graphs represent the results of pooled sample values. Similarly, the calculated p values ($p=0.587$ for alpha rods; $p=0.550$ for paranuclear rods; $p=0.427$ for cones) for the number of SRs per terminal profile, indicated that there was no significant difference in this parameter based on sample time or neonatal age.

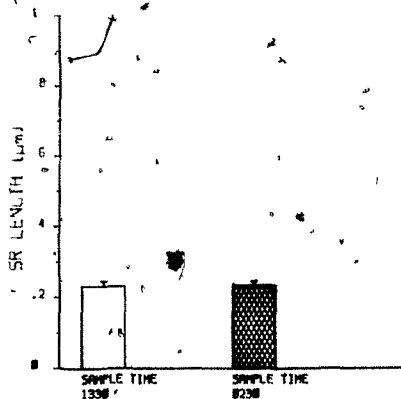
36a NEONATAL ALPHA ROD
SYNAPTIC RIBBON LENGTH



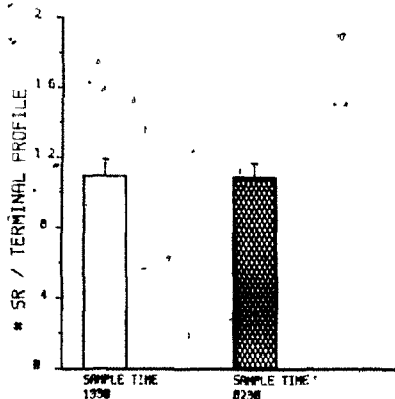
36b NEONATAL ALPHA ROD
SYNAPTIC RIBBON NUMBER



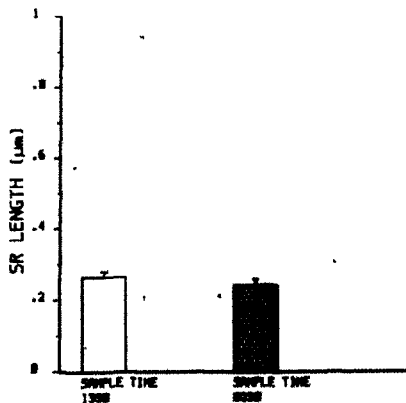
36c NEONATAL PARANUCLEAR ROD
SYNAPTIC RIBBON LENGTH



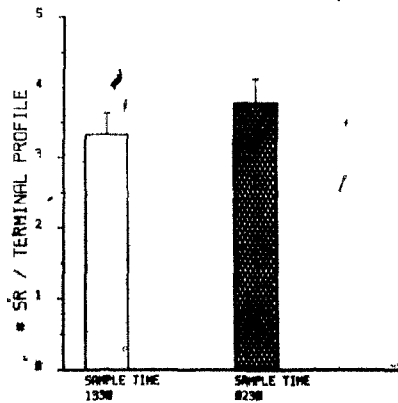
36d NEONATAL PARANUCLEAR ROD
SYNAPTIC RIBBON NUMBER



36e NEONATAL CONE
SYNAPTIC RIBBON LENGTH



36f NEONATAL CONE
SYNAPTIC RIBBON NUMBER



IV. DISCUSSION

The process of defining the presence of specific morphological changes in cells usually requires the accurate estimation of structural parameters. The quantification of these parameters, while highly desirable, is extremely labour intensive, and is dependent on a variety of extrinsic factors. One such factor that must be considered is the effect of electron microscope preparation techniques on delicate biological tissue. Tissue distortion following aldehyde fixation, dehydration and plastic embedding is a major problem that has been quantified (Arbuthnott, Ballard, Boyd and Kalu, 1980; Berthold, Corneliuson and Rydmark, 1982; Schnepf and Schnepf, 1971; Schnepf, Schnepf and Spaan, 1971) and shown to result in an approximately 10% shrinkage of mammalian nervous tissue. Since the synaptic terminals in this study were compared at the various sample times for relative, rather than absolute change, any possible error induced through tissue shrinkage (assuming it to be constant for all samples) caused by fixation and/or embedding procedures should not be a contributing factor in the final analysis. However, differential tissue shrinkage or

alternatively swelling, among the various sample times, could adversely affect data analysis. This latter possibility was controlled for in the present study by a careful monitoring of fixative osmolarity and the implementation of standardized dehydration and embedding protocols.

Sampling design is also an extremely important factor when considering the interpretation of morphometric data. Accordingly, the sampling protocol chosen for this study was a multilevel or cascade sampling design (Cruz-Orive and Weibel, 1981), where the first level was the animal, the second was eyes (left and right) from the animals, and finally, the photoreceptor synaptic terminals (from each eye of each animal). Since it has already been established (Gundersen and Osterby, 1981; Gupta, Mayhew, Bedi, Sharma and White, 1983; Mayhew, White and Gohari, 1982; Shay, 1975) that biological variation is generally the largest source of variance in such data, the statistical analysis employed must then take this into consideration. Since often it is not possible to acquire samples of equal size, especially when dealing with biological materials, the statistical analysis should compensate for unequal sample sizes as well (Kornegay and Poole, 1983). The BMDP-3V computer-based statistical package used in this study meets all of these criteria by employing a mixed model of variance and co-variance which takes into account the effect of variations among the different animals and between the eyes of each animal, on the parameter being measured.

A. Photoreceptor Synaptic Terminals

Alterations in the size and shape of photoreceptor synaptic terminals as they relate to the phenomenon of membrane turnover, have been demonstrated in a variety of vertebrates (Ball and Dickson, 1983; Cooper and McLaughlin, 1982; Scheaffer and Raviola, 1976), but rigorous quantitative (morphometric and statistical) evaluations have rarely been carried out (Ball and Dickson, 1983; Wagner, 1980). In the present study, computer-assisted morphometrics have been employed to evaluate guinea pig photoreceptor synaptic-terminal morphology during normal diurnal lighting events, and under conditions of extended light and extended darkness.

The first reports of vesicular profiles within neuronal synaptic terminals (DeRobertis and Bennett, 1954; Palade, 1954; Palay, 1954) and the evidence for the quantal release of transmitter substance (Del Castillo and Katz, 1954), led to the original proposal which linked vesicle exocytosis to transmitter release at the neuromuscular junction (Del Castillo and Katz, 1955). This theory has since been expanded to account for both the correlation of the number of quanta of transmitter released through fusion (Heuser and Reese, 1973; Heuser et al., 1979; Zimmerman, 1978; 1979a, b), with complete incorporation of the vesicle membrane into the presynaptic membrane (Heuser and Reese, 1980), and the recycling of vesicle membrane through endocytosis (Heuser and Reese, 1973). Synaptic vesicle membrane recycling

within the terminal membrane pool (synaptic vesicles, agranular endoplasmic reticulum, large smooth membrane cisternae and terminal plasmalemma) has also been shown to occur in photoreceptor synaptic terminals. Evidence for exocytotic fusion of synaptic vesicles with the presynaptic membrane has been demonstrated both in thin-section studies (Ball and Dickson, 1983; Tsukamoto, 1983) and in freeze-fracture studies (Cooper et al., 1983; Raviola and Gilula, 1975; Schaeffer and Raviola, 1976; 1978). The occurrence of endocytosis has been demonstrated in dark-adapted retinal photoreceptor synaptic terminals by the uptake of the extracellular tracer horseradish peroxidase (Cooper and McLaughlin, 1983; Ripps et al., 1976; Schacher et al., 1974; 1976; Schaeffer and Raviola, 1978). Further, this uptake process has been shown to be mediated by coated vesicles (Ball and Dickson, 1983; Cooper and McLaughlin, 1983; Schacher et al., 1976; Schaeffer and Raviola, 1976; 1978) and also by uncoated vesicles at sites near the active synaptic zones* within the terminal (Cooper and McLaughlin, 1983; Cooper et al., 1983). Therefore, the

* Couteaux and Pecot-Dechavassine (1970) originally defined an active zone in neuromuscular junctions as a specialized area of nerve terminal located directly across from a fold in the postsynaptic membrane and characterized by a density next to the presynaptic membrane and an accumulation of synaptic vesicles. The equivalent area in the photoreceptor synaptic terminal is the synaptic ridge, including the synaptic ribbon with its associated synaptic vesicles (Schaeffer, Raviola and Heuser, 1982).

inclusion of synaptic vesicle membrane within the photoreceptor synaptic terminal membrane pool must be considered when discussing changes in terminal size and shape.

Fluctuations in the size of photoreceptor synaptic vesicles have also been evaluated. The potential for vesicle size to fluctuate has been an important consideration, since De Robertis and Franchi (1956) initially reported a decrease in photoreceptor synaptic vesicle size in albino rabbits kept in constant darkness for nine days, as compared with animals exposed to sunlight. However, these findings were later disputed by the studies of Mountford (1963) and Cragg (1969), which showed no difference in the diameter of photoreceptor synaptic vesicles in terminals sampled either under light or dark conditions. These later findings are in complete agreement with the results of the present stereological study, which has shown that in the guinea pig, the mean vesicle diameter does not undergo any statistically significant change in response to a diurnal lighting cycle.

Although photoreceptor synaptic-vesicle size does not appear to change on a diurnal basis, synaptic-vesicle density has been shown to vary over 24 hrs in this and in other studies (Cragg, 1969; Schaeffer and Raviola, 1976). Since there is substantial evidence that vertebrate photoreceptors depolarize and maximally release transmitter in the dark (Dowling, 1974; Kaneko, 1979; Kaneko and

Shimizaki, 1975; Trifonov, 1968; Trifonov, Byzov and Chailahian, 1974), it is not surprising that studies have found a decrease in absolute vesicle numbers in the dark (Cragg, 1969; Schaeffer and Raviola, 1976). However, when Cragg (1969), and Ball and Dickson (1983) take into account terminal size (volume) fluctuations, the synaptic vesicle population in photoreceptor terminals appears to remain stable during a diurnal cycle. Results from the present study are in partial agreement with those of Cragg (1969), in that during the light period of a normal diurnal cycle, vesicle packing density (number of synaptic vesicles/ μm^2) was significantly greater in all three synaptic-terminal types in the adult guinea pig retina. However, our results differ from Cragg's (1969) findings of terminal size decrease in the light; on the contrary, the synaptic terminals of all three photoreceptor cell types in the guinea pig retina increased significantly in area during the light period of the diurnal lighting cycle. Thus, when both terminal area and vesicle packing density are considered together, the actual number of synaptic vesicles per terminal profile in the guinea pig was found to vary considerably over time, with far fewer vesicles being present in the dark. The result of this is, that unlike the situation described in other studies (Cragg, 1969) where vesicle depletion in the dark with subsequent membrane addition to the terminal plasmalemma is used to account for noted increases in terminal area, in the present study,

terminal area increases actually occurred in the light, and as such, appear to be independent of vesicle exocytosis.

Synaptic vesicle exocytosis in photoreceptors has not only been associated with increased terminal perimeter, but also with a decrease in the amount of plasmalemmal infolding, as well, with the result that synaptic terminals in the newt retina become more rounded in the dark (Ball and Dickson, 1983). Our results however, have indicated that although both the vesicle numerical density and the actual number of vesicles per terminal profile are decreased in the dark, a compensatory decrease in the amount of infolding, as is suggested to occur in the newt by Ball and Dickson (1983), does not take place in the guinea pig; rather, there was a significant increase in terminal plasmalemmal infolding in the dark. However, perimeter measurements from both types of rods in this study did show a significant increase during the dark period of the diurnal lighting cycle, and this could be accounted for, at least in part, by the addition of membrane to the terminal plasmalemma through vesicle exocytosis. Further, if this vesicle membrane addition were to be localized to sites immediately adjacent to processes of the postsynaptic elements, such as has been suggested by Brandon and Lam (1983), the terminal perimeter could be substantially increased simply by increasing the amount of plasmalemmal infolding at these localized sites, and without significantly increasing the overall synaptic terminal area. Alternatively, the perimeter measurements for cone

terminals, while seeming to show trends similar to those found in rods, did not demonstrate any statistically significant diurnal changes. This lack of significant perimeter change in cone terminals may, however, be accounted for by the complex shape of the cone synaptic pedicle, the numerous invaginations of postsynaptic element which enter at a variety of angles, and the larger surface area of cone terminals as compared to rods (McCartney and Dickson, 1984). In fact, the ratio of membrane added through exocytosis at specific localized sites adjacent to the postsynaptic invagination, over the total synaptic terminal membrane surface area, would in all likelihood be much greater for rod terminals than for cone terminals. Therefore, when considering the total amount of terminal membrane, these relatively small additions of vesicle membrane to the total terminal membrane surface area, should be more readily detected in rods, through perimeter measurements, where they would not be masked by a large terminal size. However, cone area and shape determinations should not be subjected to this dampening effect, since changes in these two parameters appear not to be localized to one area of the terminal plasmalemma.

Although the plasmalemma of guinea pig photoreceptor synaptic terminals clearly underwent changes both in length and infolding over 24 hrs, it would appear that the direct processes of synaptic vesicle membrane addition (exocytosis) and retrieval (endocytosis) can not completely account for

these changes, as terminals appeared larger and rounder at the same time when synaptic vesicle numerical density was also highest. Alternatively, membrane diverticula, which are believed to form as a result of synaptic vesicle exocytosis, and to function as membrane 'storage areas', have been described by Cooper and McLaughlin (1982) and Cooper et al. (1983), where they have been implicated in synaptic-terminal membrane alterations in chick photoreceptors exposed to a diurnal lighting cycle.

Although structures which superficially resembled these diverticula were observed in guinea pig photoreceptor synaptic terminals in the dark, on closer examination of serially-sectioned tissue, and after using three-dimensional reconstructions, these elaborations were shown simply to be profiles of deeply invaginated postsynaptic elements (McCartney and Dickson, 1984). Therefore, it would appear that neither the direct processes of exocytosis and endocytosis of synaptic vesicles nor the recycling mechanism proposed for chick photoreceptor synaptic terminals (Cooper and McLaughlin, 1982; 1983; Cooper et al., 1983), adequately account for the alterations in size and shape of mammalian photoreceptor synaptic terminals observed in the present study.

A mechanism which may, however, explain the light mediated size and shape changes which occur in guinea pig photoreceptor synaptic terminals, involves a system of cross-striated fibrils which have been shown in guinea pigs

to extend from the ciliary rootlet of the inner segment down through the perikaryon and into the synaptic terminal of both rods and cones (Spira and Milman, 1979). These fibrils have been noted in a variety of other mammals as well, including developing and mature mouse (Olney, 1968), adult cat (Stevens et al., 1984), and man (Villegas, 1964; Uga et al., 1970). Although their function has not been conclusively resolved, it has been suggested that they have contractile properties. Drenckhahn and Groschel-Stewart (1977) demonstrated that these fibrils in the rat photoreceptor inner segment have actin- and myosin-like activity, while Matsusaka (1967) has localized ATPase activity to the striated ciliary rootlet in the inner segments of human rods. In addition, Spira and Milman (1982) observed positive ATPase staining in these fibrils in guinea pig photoreceptors and conclude that this histochemical evidence is consistent with an energy utilizing contractile system. More recently, Stevens et al. (1984) employing computer-assisted three-dimensional reconstructions from thin sections, have demonstrated that cat photoreceptor cross-striated fibrils form a ring-like configuration within the synaptic terminal surrounding the synaptic ribbons and associated processes of invaginating postsynaptic elements. Accordingly, Stevens et al. (1984) suggested that contraction and relaxation of this ring may lead to changes in the size and shape of photoreceptor synaptic terminals.

It is now established that photoreceptors depolarize maximally in the dark (Dowling, 1974; Kaneko, 1979; Kaneko and Shimizaki, 1975; Trifonov, 1968; Trifonov et al., 1974) and if, as in other neurons, depolarization increases the rate of transmitter release, maximum contact with postsynaptic elements would provide the largest area for the transmitter to interact with the postsynaptic membrane. Changes in photoreceptor synaptic-terminal morphology could then serve to maximize the relationship of terminal plasmalemma with the invaginating processes of inner retinal neurons. This increase in surface area contact, if effected through the deeper penetration of postsynaptic elements, should be reflected in increased terminal membrane infolding and so would be evident as a reduction in photoreceptor synaptic terminal form factor measurements in the dark. Concentric contraction of the cross-striated fibril during the dark could also subserve this process by effecting a downward (vitreal) folding of the terminal plasmalemma over the processes of the postsynaptic elements, and in effect causing them to become more deeply invaginated into the receptor synaptic terminal while at the same time resulting in an increased terminal profile area. Conversely, the observed increased sectional area and decreased infolding in guinea pig photoreceptor synaptic terminals in the light may be brought about through a relaxation of this ring. By utilizing this proposed mechanism, the photoreceptor synaptic terminal could provide maximum surface area contact

with the postsynaptic cell processes during the appropriate period of the diurnal cycle.

Whether this proposed fibril-bundle mechanism is controlled by a light stimulus (on/off), or is due to some ongoing biological variation which is independent of the lighting conditions is difficult to assess directly. It was, however, possible to evaluate the effect of extended periods of continuous light or darkness on synaptic terminal morphology. It was hypothesized that if the noted alterations in photoreceptor synaptic terminal size and shape were independent of the lighting cycle, they should not be affected by continuous lighting conditions and would be maintained at or very close to the values obtained in a L:D cycle. However, in view of previous reports (Anderson, Coyle and O'Steen, 1972; Fifikova, 1972; Grignolo, Orzalesi, Castellazo, and Vitone, 1969; Kuwabara, 1970; Kuwabara and Gorn, 1968; O'Steen, Shear and Anderson, 1972; Shear, O'Steen and Anderson, 1973), which have shown that constant low-level illumination can have deleterious effects on photoreceptors, we were concerned that the planned experiment might not be feasible. Fortunately, other studies on the frog (Osborne and Monaghan, 1976) and chick (Cooper and McLaughlin, 1982), employing similar experimental conditions, produced none of these degenerative changes; similarly, no such effects were observed in any of the guinea pigs retinas used in this study. The photoreceptor synaptic terminals from the extended light

experiments appeared qualitatively similar to those sampled during diurnal cycles, and therefore the parameter measurements obtained were compared directly to those values obtained at similar sample times, but from the cycled light experiments. Morphometric measurements from both extended dark and long-term light experiments indicated that there was no significant difference between samples taken at 0600 (normal dark period in a diurnal cycle) and at 0800 (normal light period in a diurnal cycle), despite the fact that there was a statistically significant difference in receptor terminal morphology between these two sample times in animals subjected to a diurnal lighting cycle. In addition, none of the terminal measurements from the extended light or dark regimes approached values obtained in animals under a 12:12 L:D cycle and sampled at 0800. Therefore, the proposed mechanism controlling these alterations noted in a diurnal cycle, appears to be initiated, or at least enhanced, by a light stimulus rather than some internally controlled biological clock.

Further evidence in support of a light-regulated control mechanism for synaptic-terminal alterations, rather than one that is internally controlled, comes from our fetal data. Cyclic shedding of outer-segment discs was first shown by LaVail (1976) in the rat retina. Subsequent studies have established that shedding is controlled by a mechanism located within the eye (Besharse, Terrk and Dunis, 1980; Heath and Basinger, 1983; Hollyfield and Basinger, 1978;

Teirstein, Goldman and O'Brien, 1980) and, while amphibian outer segment disc shedding is tightly entrained to light onset and does not persist in extended lighting conditions (Hollyfield and Basinger, 1978; Basinger and Hollyfield, 1980; Basinger and Hoffman, 1982), outer segment disc shedding in mammalian retinas has been reported to be controlled by an ongoing biological process, even in the absence of light (LaVail, 1980; Teirstein et al., 1980). The outer segments of fetal guinea pig photoreceptors have been shown to be shed in utero (Spira and Huang, 1978) and to follow a cyclic pattern similar to the adult (Huang et al., 1982). It has been suggested that this shedding phenomenon is regulated independently from the shedding cycle of the adult, and is not under the control of maternal humoral factors (Huang et al., 1983). Results obtained in this study, from functionally mature fetal guinea pig retinas have indicated that unlike the adult, fetal photoreceptor synaptic terminals do not follow a pattern of diurnal morphological variations. While we can offer no explanation for the significant changes in two parameters (cone terminal profile area and alpha rod form factor) at two quite different and apparently unrelated times during the cycle, there does not appear to be any significant sustainable pattern of change established in fetal terminals. Therefore, it would appear that although an internally regulated process is thought to control disc shedding in utero (Huang et al., 1983), an internally

regulated process appears not to be involved in effecting the observed cyclic changes in photoreceptor synaptic terminals in the guinea pig retina.

In view of the demonstrated cyclic activity that exists in adult photoreceptor synaptic terminals, and the fact that no such activity can be demonstrated in fetal tissue, it was of interest to ascertain at what postnatal stage this activity became evident. The results which we have obtained from the morphometric determinations on neonatal retinas are, at best, ambiguous. In the adult, synaptic terminals sampled from the mid-dark period were smaller in sectional surface area than those terminals sampled during the early light period (see Fig. 13). However, a few hours later (mid-light period), area values were beginning to decline towards those values obtained in the dark. Since neonatal samples were unfortunately only taken at times (0230 - mid-dark and 1330 - mid-light) when the differences in adult tissue were inconspicuous, the values obtained for neonatal photoreceptor synaptic terminals could indicate: either that the differences in neonatal receptor terminals sampled during the light and dark period are not as pronounced as in adult retinas; or the neonatal photoreceptor synaptic terminals may show a pattern, but similar to results obtained for outer disc shedding in fetal retinas (Huang et al., 1983), it is out of phase with the adult pattern. The resolution of this question clearly requires further investigation.

Therefore, the present study has shown that guinea pig photoreceptor synaptic terminals undergo alterations in size and shape when the animals are maintained under diurnal lighting conditions. While alterations in perimeter measurements during the dark may be explained using the vesicle recycling hypothesis, the rounder and larger terminal profiles observed in the light period can not. It is suggested that a cross-striated fibril system found in all three photoreceptor cell types of the guinea pig retina as well as the photoreceptors of other mammalian retinas, may be responsible for these latter alterations. Further, data obtained from long-term light- and dark-adapted adult retinas and functionally mature fetal retinas has led us to suggest that these morphological alterations may be initiated, or at least enhanced, by a light stimulus.

B. Photoreceptor Synaptic Ribbons

Contrary to previously published reports (Spadaro et al., 1978; Wagner, 1973; Wagner and Ali, 1977) stating that variation in synaptic ribbon length and number per terminal occurs during a normal light:dark cycle, the present study has demonstrated no statistically significant change in either of these parameters in guinea pig retinal photoreceptors during a diurnal cycle. In an effort to explain why the results differ from those of others (Spadaro et al., 1978; Wagner, 1973; Wagner and Ali, 1977),

computer-generated three-dimensional reconstructions of synaptic ribbons and receptor terminals were undertaken. These 3-D reconstructions indicate that the SR should be considered to have a thickness, as well as width and length. In the present study, we have designated the distance from the arciform density to the scleral end of the SR profile as it appears in thin sections, to be the width of this organelle. This parameter has previously been termed length by others (Spadaro et al., 1978; Wagner, 1973; Wagner and Ali, 1977), but when the organelle's three-dimensional form is taken into consideration, it is apparent that width is the more appropriate descriptive term. Data comparisons with the length measurements from previous studies are valid however, as the same dimension has been evaluated in our morphometric measurements.

In this study, three-dimensional reconstructions have confirmed the basic curved shape of the alpha rod synaptic ribbon as it was first proposed by Sjöstrand in 1958; they have also demonstrated that synaptic ribbons in paranuclear rods, as well as cones, have this same basic shape. Slight variations in ribbon contour within and between receptor terminals can be explained on the basis that postsynaptic elements vary in shape and arrangement between terminals, and because the depth of penetration of postsynaptic elements has been shown to vary throughout the diurnal lighting cycle (Ball and Dickson, 1983; Brandon and Lam, 1983; Cooper and McLaughlin, 1982; Raynauld et al., 1979;

Schaeffer and Raviola, 1976; Wagner, 1980).

In reconstructed cone terminals, ribbon shape appears to be highly variable (Fig. 28). However, these variations in SR appearance should not necessarily be interpreted as changes in the true structural shape of the ribbon. Rotations of a single SR (Figs. 29 and 30) clearly demonstrated that the viewing perspective is an important consideration when interpreting this complex organelle. This is especially important in cone terminals where SRs assume a myriad of orientations.

As demonstrated here, the effect of sectioning angle on synaptic ribbon 'length' (width) can be substantial. Figure 32 shows only one of a wide range of possible sectioning angles that Grun (1980) suggested could result in an artifactual increase in SR length. In addition, since the shape of the synaptic ribbons in guinea pig photoreceptor terminals is convoluted in numerous planes, this effect would be even more pronounced than in the plate-shaped models (Bunt, 1971; Gray and Pease, 1971; McLaughlin and Boykins, 1977; Raviola and Gilula, 1975) that Grun (1980) discussed. In the present study, this potential problem was controlled for by the use of sampling criteria which ensured that rod ribbons were only sectioned perpendicularly through their width, while the vast majority of cone SRs were also sectioned perpendicular as indicated by the alignment with the synaptic ridge and the presence of the arciform density.

Sectioning angle may also have an effect on synaptic

ribbon profile shape. Isolated granular synaptic ribbons such as those reported by Spadaro et al. (1978) were never noted in guinea pig terminal profiles that met our sampling criteria. Granular profiles were noted however, in serial sections that were being used for three-dimensional reconstruction of synaptic terminals. When these terminals were reconstructed, the granular profiles always became part of synaptic ribbons. If a section were to be taken so that the synaptic ribbon was cut en face at its periphery, a round granular appearance could be generated and it would appear similar to those suggested by McLaughlin and Boykins (1977). Therefore, at least in the three photoreceptor synaptic-terminal types of the guinea pig retina, sectioning artifacts could in all likelihood account for the "granular" synaptic ribbons reported by others.

Bunt (1971) proposed that the synaptic ribbon may function to support or maintain the synaptic ridge in relation to the postsynaptic elements and in addition, or alternatively, may serve as orienting structures for a "sliding vesicle" mechanism of transmitter release. The SR would therefore have a similar function to the dense projections of brain synapses, namely to guide vesicles to a narrow strip of presynaptic membrane (Gray and Pease, 1971). Since vertebrate retinal photoreceptors have been shown to depolarize and release neurotransmitter in the dark (Dowling, 1974; Kaneko, 1979; Kaneko and Shimizaki, 1975; Trifonov, 1968; Trifonov et al., 1974), it has been

suggested (Spadaro et al., 1978; Wagner, 1973; Wagner and Ali, 1977) that fluctuations in SR length and numbers are closely related to the physiological state of the photoreceptor terminal. The formation, in the dark, and the degradation, in the light, of SRs would therefore provide increased numbers of "conveyor belts" (Bunt, 1971) at the appropriate time for transmitter release. Our results, indicated that this degradation and reformation of SRs does not occur in guinea pig photoreceptor synaptic terminals. These findings, however, do not necessarily discount the proposed explanation of SR function. If SRs do function as Bunt (1971) suggests, vesicles must be 'aligned' throughout a diurnal cycle in order to react to lighting changes. The rate at which these vesicles associate with the SR may vary throughout the cycle, but SR 'length' would not necessarily have to change in order to react to the physiological activity of the synapse.

Our findings have demonstrated that in the adult, fetal and neonatal guinea pigs there was no significant change in either synaptic ribbon 'length' or number per photoreceptor terminal during a normal 12:12 diurnal lighting cycle or in adult animals exposed to an extended light or dark regime. We have also demonstrated using computer-generated 3-D reconstructions that the synaptic ribbon is horseshoe-shaped with folds in numerous planes conforming to the invaginating postsynaptic elements.

In conclusion, the present study has provided precise statistical evaluation of the alterations that occur in guinea pig photoreceptor synaptic terminals exposed to a diurnal lighting cycle. Alterations in rod synaptic terminal perimeters, during the dark period of a diurnal cycle, may be explained using the vesicle recycling hypothesis of Heuser and Reese (1973). The noted variations in synaptic terminal size and shape in both rods and cones during the light period of a diurnal lighting cycle, however, may be effected by an annular configuration of cross-striated fibrils that are found in guinea pig and other mammalian photoreceptors. Results from experiments where extended lighting conditions were used, suggest that this cross-striated fibril mechanism may be initiated, or at least enhanced, by a light stimulus rather than some internally controlled biological clock. In addition, the combination of computer-assisted three-dimensional reconstructions and morphometric analyses has been shown to be an effective tool in providing evidence that previously reported variations in synaptic ribbon length and number per terminal profile in other vertebrates, does not occur in guinea pig photoreceptors. As result of our studies, it is apparent that the implementation of stringent sampling criteria is essential to the success of any morphometric procedure.

V. SUMMARY

1. Adult Hartley-outbred guinea pigs were entrained to a 12 hr light: 12 hr dark diurnal lighting regime for at least two weeks prior to the initiation of experiments.

2. A continual supply of fetal guinea pigs was maintained by establishing a breeding colony of adult animals. Fetal animals were obtained on the 62 ± 1 days of gestation. Fetal age was verified by using the aging criteria established by Draper (1920).

3. Neonatal animals were obtained from breeding colony stock. These animals were sacrificed at 1, 3, 5 and 7 days of age. The age at the time of sacrifice was based on equating the animal's first light period of a diurnal cycle with 1 day of age.

4. Adult, fetal and neonatal retinas were sampled at various times throughout a normal 12:12 L:D diurnal lighting cycle. Additional adult animals were entrained to long-term light (L:L) or alternatively long-term dark (D:D) before being sacrificed after 2, 7, or 14 days in the extended

lighting conditions.

5. Representative samples from all retinal quadrants were obtained and processed for electron microscopy. Computer-assisted three-dimensional reconstructions from serial thin sections were produced for all three types of synaptic terminals in order to; 1) establish standard sampling criteria; 2) visualize terminal size and shape changes; 3) show the relative position of the synaptic ribbon(s) within the terminal; and 4) show the relationship of the synaptic ribbon(s) to the invaginating postsynaptic cell processes.

6. The synaptic terminals of all three photoreceptor cell types found in this retina (alpha and paranuclear rods, and cones) were analysed using computer-based morphometrics for changes in their area, perimeter, synaptic vesicle density, degree of plasmalemmal infolding, as well as for synaptic ribbon length and number per terminal profile.

7. Analyses of adult diurnal data, using the computer-based statistical package BMDP employing a mixed model of variance and co-variance, showed that all three photoreceptor synaptic terminal types had increased area and decreased membrane infolding during the light period, while the perimeter of the rod terminals increased in the dark.

8. Results from the adults maintained in extended lighting conditions showed no statistically significant differences between sample times at which statistically significant differences clearly existed during a diurnal lighting cycle.

9. Diurnal data from fetal retinas showed no significantly sustainable pattern while neonatal animals showed no statistical difference between the light and dark sample times or between neonatal age.

10. Three-dimensional reconstructions of photoreceptor synaptic ribbons revealed that guinea pig synaptic ribbons are horseshoe-shaped with pleats in numerous planes conforming to the invaginating postsynaptic elements.

11. Morphometric data for synaptic ribbon length and number per terminal profile from diurnal and extended lighting conditions exhibited no statistically significant changes in these parameters in adult, fetal or neonatal animals.

12. These quantified findings have led to the following conclusions:

i) the alterations in rod synaptic terminal perimeter during the dark period of a diurnal cycle may be explained using the vesicle recycling hypothesis.

ii) the changes in synaptic terminal size and shape during the light period of a diurnal lighting regime may be effected by an annular configuration of cross-striated fibrils found within these terminals.

iii) the proposed cross-striated fibril mechanism appears to be initiated, or at least enhanced, by a light stimulus.

iv) the guinea pig synaptic ribbon is horseshoe-shaped and can be thought of as having a finite thickness, width (which other authors have termed length) and an overall length.

v) contrary to reports for other vertebrates, guinea pig synaptic ribbons showed no significant differences in 'length' or number per terminal profile when the retinas were exposed to normal diurnal or extended lighting conditions in adult, fetal or neonatal animals.

vi) morphometric evaluation of such parameters as synaptic terminal size and shape and synaptic ribbon length and number per terminal profile must include the implementation of stringent sampling criteria.

REFERENCES

Abercrombie, M. (1946) Estimation of nuclear population from microtome sections. *Anat. Rec.* **94**:239-247.

Anderson, K.V., Coyleand, F.P. and O'Steen, W.R. (1972) Retinal degeneration produced by low intensity light. *Exp. Neurol.* **35**:233-238.

Arbuthnott, E.R., Ballard, K.J., Boyd, I.A. and Kalu, K.U. (1980) Quantitative study of the non-circularity of myelinated peripheral nerve fibers in the cat. *J. Physiol.* **308**:99-123.

Ball, A.K. and Dickson, D.H. (1983) Diurnal variation in the photoreceptor synaptic terminals of the newt retina. *Am. J. Anat.* **168**:305-320.

Basinger, S.F. and Hoffman, R.T. (1982) Regulation of rod shedding. In "The Structure of the Eye.", Hollyfield, J.G., ed. New York, Elsevier-North Holland pp. 75-84.

Basinger, S.F. and Hollyfield, J.G. (1980) Control of rod shedding in the frog retina. *Neurochem.* **1**:81-92.

Berthold, C.H., Corneliuson, O. and Rydmark, M. (1982)
Changes in shape and size of rat spinal root myelinated
nerve fibers during fixation and Vestopal-W embedding
for electron microscopy. J. Ultrastruc. Res. **80**:23-41.

Besharse, J.C., Terrk, R.O. and Dunis, D.A. (1980) Light
evoked disc shedding by rod photoreceptors in
vitro. Invest. Ophthalmol. Vis. Sci. **19**:1512-1517.

Brandon, C. and Lam, D.M.K. (1983) The ultrastructure of rat
rod synaptic terminals: Effects of dark-adaptation.
J. Comp. Neurol. **217**:167-175.

Bunt, A.H. (1971) Enzymatic digestion of synaptic ribbons in
amphibian retinal photoreceptors. Brain Res. **25**:571-
577.

Cohen, A.I. (1960) The ultrastructure of the rods of the
mouse retina. Am. J. Anat. **107**:23-48.

Cooper N.G.F. and McLaughlin, B.J. (1982) Structural
correlates of physiological activity in chick
photoreceptor synaptic terminals: Effects of light and
dark stimulation. J. Ultrastruc. Res. **79**:58-73.

Cooper, N.G.F. and McLaughlin, B.J. (1983) Tracer uptake by photoreceptor synaptic terminals. I. Dark mediated effects. J. Ultrastruc. Res. **84**:252-267.

Cooper, N.G.F., McLaughlin, B.J. and Boykins, L.G. (1983) Synaptic membrane domains in photoreceptors of chick retina: A thin section and freeze-fracture study. J. Ultrastruc. Res. **82**:172-188.

Couteaux, R. and Pecot-Dechavassine, M. (1970) Vesicules synaptiques et poches au niveau des " zones actives " de la jonction neuromusculaire. Comptes Rendus Hebdomadaires des Seances de l'Academie des Sciences Series D **271**:2346-2349.

Cragg, B.G. (1969) Structural changes in naive retinal synapses detectable within minutes of first exposure to daylight. Brain Res. **15**:79-96.

Cruz-Orive, L.M. and Weibel, E.R. (1981) Sampling designs for stereology. J. Microsc. **122**:235-258.

Del Castillo, J. and Katz, B. (1954) Quantal components of the end-plate potential. J. Physiol. **124**:560-573.

Del Castillo, J. and Katz, D. (1955) Local activity at a depolarized nerve-muscle junction. J. Physiol. 128: 396-411.

De Robertis, E.D.P. and Bennett, H.S. (1954) Submicroscopic vesicular component in the synapse. Fed. Proc. 13:35a

De Robertis, E. and Franchi, C.M. (1956) Electron microscope observations on synaptic vesicles in synapses of the retinal rods and cones. J. Biophysic. and Biochem. Cytol. 2:307-318.

Dowling, J.E. (1974) Synaptic arrangements in the vertebrate retina: The photoreceptor synapse. In "Synaptic Transmission and Neuronal Interactions". M.V.L. Bennet, ed. Raven Press, New York, pp. 87-103.

Draper, R.L. (1920) The prenatal growth of the guinea pig. Anat. Rec. 18:369-392.

Drenckhahn, D. and Groschel-Stewart, U. (1977) Localization of myosin and actin in ocular nonmuscle cells: Immunofluorescence-microscopic, biochemical and electron microscopic studies. Cell Tissue Res. 181:493-503.

- Dunant, Y. and Israel, M. (1979) When the vesicular hypothesis is no longer the vesicular hypothesis. Trends Neurosci. 2:130-133.
- Fatt, P. and Katz, B. (1952) Spontaneous subthreshold activity at motor nerve endings. J. Physiol. London. 117:109-128.
- Fifkova, E. (1972) Effect of light and visual deprivation on the retina. Exp. Neurol. 35:450-457.
- Fine, B.S. (1962) Synaptic lamellae in the human retina: An electron microscope study. J. Neuropath. Exp. Neurol. 22:255-262.
- Gray, E.G. and Pease, H.L. (1971) On understanding the organization of the retinal receptor synapse. Brain Res. 35:1-15.
- Grignolo, A., Orzalesi, N., Castellazo, R. and Vitone, P. (1969) Retinal damage by visible light in albino rats: An electron microscope study. Ophthalmologica 157: 43-59.
- Grun G. (1980) Development dynamic in synaptic ribbons of retinal receptor cells (Tilapia, Xenopus). Cell Tissue Res. 207:331-339.

- Gundersun, H.J.G. (1980) Stereology - or how figures for spatial shape and content are obtained by observation of structures in sections. *Microscopica ACTA* **83**:409-426.
- Gundersun, H.J.G. and Osterby, R. (1981) Optimizing sampling efficiency of stereological studies in biology: or "Do more less well". *J. Microsc.* **121**:65-74.
- Gupta, M., Mayhew, T.M., Bedi, K.S., Sharma, A.K. and White, F.W. (1983) Inter-animal variation and its influence on the overall precision of morphometric estimates based on nested sampling designs. *J. Microsc.* **131**:147-154.
- Heath, A.R. and Basinger, S.F. (1983) Frog rod outer segment shedding in vitro: histologic and electrophysiologic observations. *Invest. Ophthalmol. Vis. Sci.* **24**:177-284.
- Heuser, J.E. and Reese, T.S. (1973) Evidence for recycling of synaptic vesicle membrane during transmitter release at the frog neuromuscular junction. *J. Cell Biol.* **57**:315-344.
- Heuser, J.E. and Reese, T.S. (1980) Structural changes following transmitter release at the frog neuromuscular junction. *J. Cell Biol.* **88**:564-580.

Heuser, J.E., Reese, T.S., Dennis, M.J., Jan, Y., Jan, L. and Evans, L. (1979) Synaptic vesicle exocytosis captured by quick-freezing and correlated with quantal transmitter release. *J. Cell Biol.* **81**:275-300.

• Hollyfield, J.G. and Basinger, S.F. (1978) Photoreceptor shedding can be initiated within the eye. *Nature* **274**: 794-796.

Holtzman, E. and Mercurio, A.M. (1980) Membrane recycling in neurons and photoreceptors: Some unresolved issues. *Int. Rev. Cytol.* **67**:1-68.

Huang, P.T., Spira, A.W. and Wyse, J.P.H. (1982) Phagocytosis in the fetal pigment epithelium: Evidence for cyclic activity. *Invest. Ophthalmol. Vis. Sci.* **22**: 428-438.

Huang, P.T., Spira, A.W. and Wyse, J.P.H. (1983) Effects of alteration in the light cycle on outer segment shedding in the fetal retina. *Invest. Ophthalmol. Vis. Sci.* **24**: 857-861.

IBAS I Software Documentation, (1981) Carl Zeiss Ltd.

Kaneko, A. (1979) Physiology of the retina. *Annu. Rev. Neurosci.* **2**:169-191.

Kaneko, A. and Shimizaki, H. (1975) Effects of external ions on the synaptic transmission from photoreceptors to horizontal cells in the carp retina. *J. Physiol.* (Lond.). **252**:509-522.

Kornegay III, W.D. and Poole, M.C. (1983) A computer program using a nested analysis of variance in morphometric sampling. *Compt. Pro. Biomed.* **16**:155-160.

Kuwabara, T. (1970) Retinal recovery from exposure to light. *Am. J. Ophthalmol.* **70**:187-198.

Kuwabara, T. and Gorn, R.A. (1968) Retinal damage by visible light: An electron microscope study. *Arch. Ophthalmol.* **79**:69-78.

Ladman, A.J. (1958) The fine structure of the rod-bipolar synapse in the retina of the albino rat. *J. Biophys. Biochem. Cytol.* **4**:459-466.

LaVail, M.M. (1976) Rod outer segment disc shedding in the rat retina: Relationship to cyclic lighting. *Science* **194**:1071-1073.

LaVail, M.M. (1980) Circadian nature of rod outer segment disc shedding in the rat. *Invest. Ophthalmol. Vis. Sci.* **19**:407-411.

Marchbanks, R.M. (1978) The vesicular hypothesis questioned. *Trends Neurosci.* **1**:83-84.

Marchbanks, R.M. (1979) In reply to Dr. Whittaker. *Trends Neurosci.* **2**:56.

Mayhew, T.M., White, F.W. and Gohari, K. (1982) Towards economy of effort in quantitative ultrastructural pathology: Efficient sampling schemes for studying experimental carcinogenesis. *J. Path.* **138**:179-191.

Matsusaka, T. (1967) ATPase activity in the ciliary rootlet of human retinal rods. *J. Cell Biol.* **33**:203-208.

McCartney, M.D. and Dickson, D.H. (1984) Diurnal morphometric and 3-D reconstruction analysis of guinea pig photoreceptor synaptic ribbons. *ARVO Supp. Invest. Ophthalmol. Vis. Sci.* **25**:63.

McLaughlin, B.J. and Boykins, L. (1977) Ultrastructure of E-PTA stained synaptic ribbons in the chick retina. *J. Neurobiol.* **8**: 91-96.

Miller, T.M. and Heuser, J.E. (1984) Endocytosis of synaptic vesicle membrane at the frog neuromuscular junction.

J. Cell Biol. **98**:685-698.

Mountford, S. (1963) Effects of light and dark adaptation on the vesicle populations of receptor-bipolar synapses.

J. Ultrastruc. Res. **9**:403-418.

Mountford, S. (1964) Filamentous organelles in receptor-bipolar synapses of the retina. J. Ultrastruc. Res.

10:207-216.

Olney, J.W. (1968) An electron microscopic study of synapse formation, receptor outer segment development and other aspects of developing mouse retina. Invest. Ophthalmol. Vis. Sci. **7**:250-268.

Osborne, M.P. and Monaghan, P. (1976) Effects of light and dark upon photoreceptor synapses in the retina of Xenopus laevis. Cell Tiss. Res. **173**:211-220.

Osborne, M.P. and Thornhill, R.A. (1972) The effect of monoamine depleting drugs upon the synaptic bars in the inner ear of the bullfrog. Z. Microsk. Anat. **127**:347-355.

O'Steen, W.K., Shear, C.R. and Anderson, K.V. (1972) Retinal damage after prolonged exposure to visible light: A light and electron microscope study. Am. J. Anat. **134**: 5-22.

Palade, G.E. (1954) Electron microscope observations of interneuronal and neuromuscular synapses. Anat. Rec. **118**:335a

Palay, S.L. (1954) Electron microscope study of the cytoplasm of neurons. Anat. Rec. **118**:336a.

Raviola, E. and Gilula, N.B. (1975) Intramembrane organization of specialized contacts in the outer plexiform layer of the retina: A freeze-fracture study in monkeys and rabbits. J. Cell Biol. **65**:192-222.

Raynauld, J.P, Lavoilette, J.R. and Wagner, H.J. (1979) Goldfish retina: A correlate between cone activity and morphology of the horizontal cell in cone pedicles. Science **204**:1436-1438.

Reynolds, E.S (1963) The use of lead citrate at high pH as an electron opaque stain in electron microscopy. J. Cell Biol. **17**:208-212.

Ripps, H., Shakib, M. and MacDonald, E.D. (1976) Peroxidase uptake by photoreceptor terminals of the skate retina. J. Cell Biol. **70**:86-96.

Schacher, S.M., Holtzman, E. and Hood, D.C. (1974) Uptake of horseradish peroxidase by frog photoreceptor synapses in the dark and the light. Nature **249**:261-263.

Schacher, S.M., Holtzman, E. and Hood, D.C. (1976) Synaptic activity of frog retinal photoreceptors: A peroxidase study. J. Cell Biol. **70**:178-192.

Schaeffer, S.F. and Raviola, E. (1976) Ultrastructural analysis of functional changes in the synaptic endings of turtle cones. Cold Spring Harbor Symp. **40**:521-528.

Schaeffer, S.F. and Raviola, E. (1978) Membrane recycling in the cone cell endings of the turtle retina. J. Cell Biol. **79**:802-825.

Schaeffer, S.F., Raviola, E. and Heuser, J.E (1982) Membrane specializations in the outer plexiform layer of the turtle retina. J. Comp. Neurol. **204**:253-267.

Schmalenberger, B. (1980) Differentiation of the guinea pig eye - nuclear ultrastructure, template activity and DNA content. Protoplasma **103**:377-392.

Schnepf, P. and Schnepf, G. (1971) Analysis of peripheral nerve fibers in animals of different body size.

II. Ratio of axon diameter to fiber diameter and internodal length. Z. Zellforsch. 119:99-114.

Schnepf, G., Schnepf, P. and Spaan, G. (1971) Analysis of peripheral nerve fibers in animals of different body size. I. Total fiber count, fiber size and nerve conduction velocity. Z. Zellforsch. 119:77-98.

Shay, J. (1975) Economy of effort in electron morphometry. Am. J. Path. 81:503-511.

Shear, C.R., O'Steen, W.R. and Anderson, K.V. (1973) Effects of short-term low intensity light on the albino rat retina: An electron microscopic study. Am. J. Anat. 138:127-132.

Sjostrand, F.S. (1953) The ultrastructure of the inner segment of the retinal rods of the guinea pig as revealed by electron microscopy. J. Cell and Comp. Physiol. 42:45-70.

Sjostrand, F.S. (1958) Ultrastructure of retinal rod synapses of the guinea pig eye as revealed by three-dimensional reconstruction from serial sections. J. Ultrastruc. Res. 2:122-170.

Small, J.V. (1968) Measurement of section thickness. In "Proceedings of the 4th European Congress on Electron Microscopy". Microscopy 1:609-610.

Spadaro, A., de Simone, I. and Puzzolo, D. (1978) Ultrastructural data and chronobiological patterns of the synaptic ribbons in the outer plexiform layer in the retina of albino rats. ACTA Anat. 102:365-373.

Spira, A.W. (1975) In utero development and maturation of the retina of a non-primate mammal: A light and electron microscopic study of the guinea pig. Anat. Embryol. 146:279-300.

Spira, A.W. and Huang, P.T. (1978) Phagocytosis of photoreceptor outer segments during retinal development in utero. Am. J. Anat. 152:523-528.

Spira, A.W. and Milman, G.E. (1979) The structure and distribution of the cross-striated fibril and associated membranes in guinea pig photoreceptors. Am. J. Anat. 155:319-337.

Spira, A.W. and Milman, G.E. (1982) Filament arrays in the photoreceptor cell of the human, monkey and guinea pig. In "The Structure of the Eye." Hollyfield, J.G., ed. New York, Elsevier-North Holland, pp. 1-10.

- Stevens, J.K., Jacobs, R. and Jackson, L. (1984) Rings of cross-striated fibrils within the cat cone pedicle: A computer-assisted serial EM analysis. Invest. Ophthalmol. Vis. Sci. 25:201-208.
- Teirstein, P.S., Goldman, A.I. and O'Brien, P.J. (1980) Evidence for both local and central regulation of rat rod outer segment disc shedding. Invest. Ophthalmol. Vis. Sci. 19:1268-1273
- Trifonov, Y.A. (1968) Study of synaptic transmission between the photoreceptor and the horizontal cell using electrical stimulation of the retina. Biophysika. 13: 809-817.
- Trifonov, Y.A., Byzov, A.L. and Chailahian, L.M. (1974) Electrical properties of horizontal cells in fish retina. Vision Res. 14:229-241.
- Tsukamoto, Y. (1983) Light-related changes in electron-dense material in photoreceptor synaptic clefts of the frog, Rana catesbeinna. Cell Tissue Res. 234:579-594.
- Uga, S., Nakao, F., Mimura, M. and Ikui, H. (1970) Some new findings on the fine structure of the human photoreceptor cell. J. Elect. Micr. 19:71-84.

Villegas, G.M. (1964) Ultrastructure of the human retina.

J. Anat. 98:501-513.

Wagner, H.J. (1973) Darkness-induced reduction of the number of synaptic ribbons in fish retina. Nature New Biol. 246:53-55.

Wagner, H.J. (1980) Light-dependent plasticity of the morphology of horizontal cell terminals in cone pedicles of fish retinas. J. Neurocytol. 9:573-590.

Wagner, H.J. and Ali, M.A. (1977) Cone synaptic ribbons and retinomotor changes in brook trout, Salvelinus fontinalis (Salmonidae teleostei) under various experimental conditions. Can. J. Zool. 55:1684-1691.

Zimmermann, H. (1978) Turnover of adenine nucleotides in cholinergic synaptic vesicles of the Torpedo electric organ. Neurosci. 3:827-836.

Zimmermann, H. (1979a) Vesicular heterogeneity and turnover of acetylcholine and ATP in cholinergic synaptic vesicles. Prog. Brain Res. 49:141-151.

Zimmermann, H. (1979b) Commentary on the vesicle hypothesis. Trends Neurosci. 2:282-285.

CURRICULUM VITAE

NAME: McCartney, Mitchell David

BORN: September 3, 1955.
Guelph, Ontario

MARITAL STATUS: Married to Patricia Dianne Goodwin
November 26, 1983.

CITIZENSHIP: Canadian

EDUCATION: PRIMARY: Kindergarten - Grade IV
Grade VII - Grade VIII
King George Public School
Guelph, Ontario
1960-1965, 1967-1969

Grade V - Grade VI
Laurine Avenue Public School
Guelph, Ontario
1965-1967

SECONDARY: Grade IX - Grade XIII
John F. Ross C.V.I.
Guelph, Ontario
1969-1974

UNIVERSITY: B.Sc. (Hons.) Biological Science
University of Guelph
1974-1978

M.Sc. (Anatomy)
University of Western Ontario
1978-1980
Thesis Title : Contact Guidance:
A Comparison Between Normal and
Tumour Cells
Supervisor: Dr. R.C. Buck

Ph.D Candidate
Department of Anatomy
Dalhousie University
1980-present

DEGREES:

B.Sc. (Hons.) Biological Science
University of Guelph
1978

M.Sc. (Anatomy)
University of Western Ontario
1980

TEACHING EXPERIENCE:

Laboratory Instructor:

1978-1979 - Undergraduate Microanatomy
Department of Anatomy
University of Western Ontario

1980-1981 - Medical Microanatomy
Department of Anatomy
Dalhousie University

1981-1982 - Medical Gross Anatomy
Department of Anatomy
Dalhousie University.

1982-1983 - Medical Microanatomy
Department of Anatomy
Dalhousie University

- Medical Gross Anatomy
Department of Anatomy
Dalhousie University

1983-1984 - Medical Gross Anatomy
Department of Anatomy
Dalhousie University

- Undergraduate Anatomy
Anatomy 102C
Department of Anatomy
Dalhousie University

ADMINISTRATIVE EXPERIENCE:

Graduate Student Representative
Department of Anatomy
Dalhousie University
1982-1983

Graduate Studies Committee
Member
Department of Anatomy
Dalhousie University
1982-1983

AWARDS/PRIZES:

Dalhousie Teaching Assistantship
Dalhousie Graduate Fellowship
1980-1981

Dalhousie Graduate Fellowship
1981-Present

AFFILIATIONS:

Canadian Association of Anatomists
Member
1981-present

Microscopical Society of Canada
Member
1980-present

PUBLICATION:

ABSTRACTS:

McCartney, M.D. and Dickson, D.H.
(1983) Diurnal variations in guinea
pig photoreceptors. *Anat. Rec.* 205:
116A.

McCartney, M.D. and Dickson, D.H.
(1984) Diurnal morphometric and 3-D
reconstruction analysis of guinea
pig photoreceptor synaptic ribbons.
ARVO Supp. Invest. Ophthalmol. Vis. Sci. 25:63.

PAPERS:

McCartney, M.D. and Buck, R.C. (1981)
Comparison of the degree of contact
guidance between tumor cells and
normal cells *in vitro*.
Cancer Res. 41:3046-3051.

PAPERS SUBMITTED

McCartney, M.D. and Dickson, D.H.
Photoreceptor synaptic ribbons:
Three-dimensional shape, orientation
and diurnal (non) variation.
(Exp. Eye Res.)

McCartney, M.D. and Dickson, D.H.
Morphometric analysis of diurnal
variations in the retinal
photoreceptor synaptic terminals of
the adult and fetal guinea pig.
(Am. J. Anat.)